

HOMOGENEITY OF CVD DIAMOND DETECTORS

IN TRACKING APPLICATIONS

C. Manfredotti¹, E. Vittone, F. Fizzotti, A. Lo Giudice and R. Lu

Experimental Physics Department, University of Torino, Italy

and Sezione di Torino, INFN (National Institute for Nuclear Physics, Italy)

Abstract

Data obtained from IBIC (Ion Beam Induced Charge) measurements on CVD diamond samples “ detector grade” have been used in order to “simulate” the collection of charge produced by a minimum ionizing particle. It turns out that both the electrical field and the charge collection length are not uniform in the depth of the sample, while the profile of the charge collection efficiency is compatible with a linear behaviour of the product (mobility)x(lifetime) of carriers, which is here proposed as a new “linear model” , fully compatible with the “old” linear model in all the cases where the electric field is uniform. The contribution of electrons to the charge pulse is found to be much more important than that of holes. The homogeneity of the CVD diamond detector as tracker for minimum ionising particles is much higher than for low energy protons and it displays a behaviour as a function of bin dimension which is a relatively good agreement with data reported from measurements with diamond strip detectors.

1. Introduction

Homogeneity has been recognised as a real problem in CVD diamond nuclear detectors and it is still an argument of some debate. Microprobe measurements using both frontal and lateral IBIC (Ion Beam Induced Charge) have proved that CVD diamond response to nuclear particles is not homogeneous both in depth [1] and in detection plane [2]. The fact that charge collection efficiency for Minimum Ionizing Particles (MIPs) resulted to be dependent on the detector thickness forced the adoption of the “linear model”, which assumes a collection length linearly increasing from the substrate side [3]. But, even with MIPs, homogeneity of the charge signal in the detection plane and emerging from Landau fluctuations was questioned by some researchers [4].

The present paper will try to find some answers to the above questions and to prove the validity of the idea behind the linear model, which we propose here to substitute by a more physical one. The

¹ Contact author: Prof. Claudio Manfredotti, Experimental Physics Department, University of Torino, via Pietro Giuria 1, 10125 Torino (Italy), Tel.: +39-0116707306, Telefax: +39-0116691104, e-mail: manfredotti@to.infn.it

following topics will be presented and discussed sequentially:

- (1) Behaviour of the charge collection efficiency with respect to the polarity of the bias voltage
- (2) Effects at the electrodes
- (3) Separation of the contributions of electrons and holes
- (4) Effect of priming
- (5) Simulation of MIPs signal distribution by using micro-IBIC data
- (6) Homogeneity of collection and counting efficiencies for MIPs on charge collection efficiency

2. Experimental

For this work, we cleaved a sample particularly good from the point of view of homogeneity. The sample was 200 μm thick with a total surface area of 0.5 cm^2 and was equipped with standard Au/Cr contact on both sides.

A cleavage *cross-section* of the sample, perfectly planar, was used for micro-IBIC measurements (see [1] for details and Fig. 1 for the experimental arrangement) : a total area of 200 x 450 μm^2 was scanned by a 4 MeV proton microbeam in order to obtain collection efficiency maps at different bias voltages. The collection efficiency was obtained by comparison with a Si surface barrier detector used in the same conditions of the electronics set-up, by assuming a 100% collection efficiency.

In what follows, we will report collection efficiency profiles along the sample thickness (from which we will extract electric field and other kind of profiles) which are deduced over the total width of the sample. This is due to the fact that, in order to have very small doses to the sample delivered by incoming protons, the pulse statistics in each pixel was very low. In order to check for the representativeness of the selected area, we compared the spatial averages of collection efficiency in three regions, 150 μm wide, in which we divided the total width of the region (450 μm) and we found that fluctuations of the average values were within 5 %, confirming that the similarity of behaviour among these regions was reasonably good.

3 . Analysis of data

The “ average” efficiency curves as a function of depth were calculated over the whole selected area, as reported above, and analyzed according to a theoretical model [5] based on Ramo’s theorem, which states that the collection efficiency is a sum of two path integrals which are functions of $\mu\tau$ (mobility x lifetime product of carriers) and of the electric field. Here “depth” has the meaning of the distance from the top electrode (growth side). The averaging procedure has included, by calculation, the direction parallel to the electrodes in the cross-section plane and, for

data collection, the direction parallel to the electrodes and normal to the cross-section plane (the direction of hitting protons). In the latter case the averaging procedure is strongly affected by the energy loss mechanism for protons and it is dominated by Bragg's peak. As a consequence, the reported values of charge collection length can be considered as measured roughly at the end of proton range, i.e. a "depth" of about 75 μm .

In order to simplify the complicated process of the fitting, we made the following assumptions:

- (1) a constant ratio between $(\mu\tau)_e$ and $(\mu\tau)_h$, i.e. the sample electronic quality at a certain point reflects itself in both types of carriers.
- (2) a linear behaviour of $\mu\tau$ from back contact (substrate side) to top contact (growth side). This hypothesis coincides with the "traditional" linear model only in the case of a uniform electric field, because this last model assumes a linear behaviour of the collection length, i. e. the product of $\mu\tau E$ (where E is the electric field). From our point of view, a "physical" linear model should be related only to $\mu\tau$, since the electric field is not a crystal property by itself. At the moment, our aim is only to check if this "linear model" is compatible with our data (obviously, we used the $\mu\tau$ product which was more compatible contemporarily with all the data obtained at different bias and with different polarity). In the last paragraphs, we will show that this model is also compatible with data obtained with MIPs.
- (3) the only parameters left free to fit each curve were therefore related to the electric field. To this purpose, we use a combination of two different log-normal curves, with three parameters each : position, width and maximum height. This resulted to be the better choice with respect to all the trials carried out so far.

4 . Effects of bias polarity

A first fit, taken over a collection efficiency profile measured at +400 V bias voltage applied to the top contact (growth side, at the left) is shown in Fig.2. The points represent the sum of the contributions of holes (open dots) and of electrons (full dots). The contribution of electrons is therefore much larger than that of holes, as indicated by the maximum shifted towards the right. In fact, the increase of collection efficiency is relatively small (from 15% to 25%), due to the decrease of collection length, and it drops in the region where the electric field starts to decrease.

Fig.3 reports the behaviour of the various parameters: the top value of $(\mu\tau)_e$ is almost $0.55 \times 10^{-6} \text{ cm}^2\text{V}^{-1}$, a quite respectable value, while for holes it is $0.05 \times 10^{-6} \text{ cm}^2\text{V}^{-1}$, with a reduction factor of almost 10. The collection length, at the top, is obviously the product of the two curves below. The decrease of $\mu\tau$ at the right is not large, with the conclusion that the back part of the sample was probably cut away, as demonstrated by a physical insight.

Fig.4 reports the same behaviour of Fig.3 for an inverted bias voltage: the maximum of collection efficiency is now increased up to more than 47% (the maximum collection length for electrons is now about 250 μm and the average about 100 μm), but it is strongly affected by the decrease of the contribution of electrons towards the right. In the same way, Fig.5 shows the behaviour of the parameters, as it was the case for Fig.3. The electric field now is much more distributed inside the sample and towards the bottom electrode at the right. Because of the complicated fitting procedure, it could well be that the exact shape is different (keeping constant the integral area under the curve), but it certainly extends over the middle of the sample, in order to allow for a contribution of holes as indicated in Fig.4

Which kind of results could be now imaged to be obtained with the same sample by using MIPs? Simply calculating the average values of collection length along the depth from the profiles shown in Fig.3 and Fig.5 (top). The results of this procedure are shown in Fig.6: the averaging procedure produces a *symmetric result* even if the microscopic data were not symmetric. This observation could be easily taken as a proof of a symmetric behaviour of the contacts, which, as previously shown, is absolutely not the case. Fig.7 shows more clearly a similar, almost symmetric behaviour for the collection length of holes. Taking now the the sum of the collection lengths, $L_e + L_h$, which is what is called collection length as measured with MIPs, one gets about 50 μm @ 1 V/ μm , which is quite reasonable for this sample. In other words, the high $\mu\tau$ product for electrons, which could in principle contribute to give larger values of the collection length in the case of the negative bias voltage, is in this case counterbalanced almost exactly by the behaviour of the electric field, which displaces itself more deeply in the sample, and it does not reproduce the same maximum at the front electrode, as it was the case for positive biases.

5 . Effects at the electrodes

Fig.8 shows the behaviour of the electric field for positive biases: 400, 500 and 600 V. The maximum at the electrode lowers and the field penetrate more deeply inside the sample. Why the sample is not totally depleted, even if displaying in fact a resistivity larger than $10^{13} \Omega \text{ cm}$, is relatively easy to explain. In fact, in order to obtain a total depletion, one must avoid the effects of charged traps, which contribute to space charge in the same way as donors and acceptors. It is easy to calculate that, in order to completely deplete a detector 200 μm thick one needs to have a trap concentration less than about $5 \times 10^{12} \text{ cm}^{-3}$, i. e. a defect or contamination level which could be reached only in germanium and silicon.

As a matter of fact, it is not a real barrier which is created, since its width seems not to be dependent on the bias voltage in a corrected way. A completely different case (see Fig.9) is reported for negative bias voltages: here in fact, apart from a small frontal region, the electric field

is spreading almost completely inside the sample and it increases up to a quasi- complete depletion at -300 V (at -400 V , the shape, as indicated before, could be due to mathematical fitting procedure and it could be easily substituted by a shape more similar to the other ones). It seems therefore that a barrier constitution either does not occur or it occurs only to a small extent. Looking at Fig.10, in fact, one can deduce only a small hole injection and trapping at the right and, for bias voltages lower than 400 V , a small negative space charge on the left, of the order of few 10^{13} cm^{-3} (in the positive bias case, the space charge is of the order of 10^{15} cm^{-3} and it is capable to sustain the whole bias voltage). Therefore, both space charges in this case affect only a small fraction of the sample on both sides, with a local reduction of collection efficiency, but still allowing for an almost complete depletion.

6 . Electrons and holes contributions to the charge collection efficiency

A not negligible result of this research, which by the way is also confirmed by other data, is related to the big difference between $(\mu\tau)_e$ and $(\mu\tau)_h$. Even if an order of magnitude of difference in $(\mu\tau)$ products between electrons and holes could be also partly due to the complexity and to the sensitivity of the fitting procedure - or even be ascribed to the investigated sample -, the predominance of electron over hole transport in CVD diamond has to be taken for sure, at least in the unprimed state. This conclusion could deserve some considerations concerning the type of trapping or recombination centres responsible for the performances of CVD diamond as a nuclear particle detector.

7 . Effect of priming

The effect of priming, as investigated by micro-IBIC, has been reported to some extent elsewhere [6]. It has been observed that priming does increase the extension of high collection efficiency regions towards the electrodes, making the sample more homogeneous with respect to transport properties and increasing also the average charge collection efficiency. Generally, the effect of priming is described as trap filling by the generated carriers. Generally, collection efficiency in the case of a standard priming treatment (with irradiation dose from 10 to 100 Gy of x-rays or electrons) increases by a factor of 1.8, as reported in literature data [7]. In what follows, we will present and discuss the effect of priming as produced and investigated by the microbeam itself.

Fig.11 shows, at the top, the map of collection efficiency as obtained by micro-IBIC, in another region close to the region investigated so far, and , at the bottom left, the map of recorded counts per pixel (please note that in this case fluctuations in the microbeam intensity could be important). Finally, the figure at the bottom right shows the multichannel spectrum.

As previously noticed, by using the microbeam itself as a priming tool, it is possible to get the IBIC maps after the priming during the experiment itself, i.e. to follow the priming effect step by step.

After a proton dose of 46 Gy, the IBIC map of collection efficiency looks as in Fig.12 (top). An increase of the average collection efficiency is directly observable and also the counts map (bottom left) is more homogeneous now (the meaning is that now less pulses fall below the electronic threshold), but , what is more astonishing, is that now the multichannel spectrum has no more an exponential tail, but a peak. As a conclusion, the sample in this “primed state” is more homogeneous.

By the same averaging procedure as described formerly, we can obtain from Fig.11 (unprimed or not irradiated case) the depth profile of the charge collection efficiency (see Fig.13, which has to be compared with Fig.4) and to fit it with the relationship calculated from Ramo’s theorem. As before, full dots indicate the electron contribution and open ones the contribution of holes, and the sum of the two (points connected by the line) is used for the fit, in which the same assumptions indicated above and the same values of $(\mu\tau)$ products were used. The goodness of the fit is a proof that the assumptions are really valid. The results of the fit in terms of charge collection profile (Fig.14, top), electric field profile (centre) and $(\mu\tau)$ products behaviour (bottom) can be compared with those reported in Fig.5 (bias voltage is -300 V in this case, but the presence of a double broad peak in the electric field profile could be ascribed to the uncertainties in the fitting, as before). The average collection length over the sample thickness is now $51.1 \mu\text{m}$ for electrons and $4.2 \mu\text{m}$ for holes (but the $\mu\tau$ behaviour is the same).

Looking now to Fig.15, which refers to the irradiated case, one observe the more homogeneous behaviour of the collection efficiency and the strong increase in its maximum value, but, as in the non-irradiated case, the contribution of electrons is still very predominant with respect to holes. Please note that fluctuations of the data are much smaller and the fit much better than before. The results of the fit are reported in Fig.16, which reports the behaviour of the collection length (top), of the electric field profile (medium) and of the $(\mu\tau)$ product (bottom). The electric field is now totally spreading in the bulk of the sample, hole injection has no visible effect and the $(\mu\tau)$ product behaviour is improved both in slope and in the absolute values. The average collection lengths are now $93.2 \mu\text{m}$ for electrons and $7.7 \mu\text{m}$ for holes respectively: it is noteworthy to observe that the ratio of the increase with respect to the irradiated case is exactly 1.82 for electrons and 1.83 for holes.

The fixed charge density profiles as obtained by differentiating the electric field profiles, are shown in the following figures. In the irradiated case (Fig.17), the flattening and the strong lowering of the space charge profile are clearly evident.

Finally, Fig.18 shows a magnified view of Fig.17 for the irradiated case. Not taking into consideration the behaviour at the extreme right, which is affected by the small flexus in the electric field profile (see Fig.16), the most prominent effect is the strong reduction of space charge at the

cathode at the left, probably due to holes generated in the bulk. The presence of a negative charge at the cathode is likely due electrons injection. As a matter of fact, the phenomena are quite complicated because of separated contributions of $(\mu\tau)$ products and of the electric field: $(\mu\tau)$ products increase now more at the back contact (a factor 3.2 with respect to a factor 1.5 at front contact), while the electric field lowers in the frontal region and largely improves in the central part of the sample. The real data are represented by the collection lengths which are slightly lower in the front (or left) region, and higher in the central and in the right region. This beneficial effect is due probably to electrons, which travels toward the right, i.e. in a region in which trap density is probably larger. A model of what happens is certainly outside of the scope of the present work and it will be left for a later moment, when other data concerning other kinds of experimental data will be available.

8 . Simulation of MIPs signal distribution by using micro-IBIC data

By the availability of maps of collection efficiency in a cross-section of the detector, it is relatively easy to simulate the pulse spectrum given by MIPs, apart, of course, from Landau fluctuations. For sake of simplicity, we shall assume a standard MIP with a uniform energy loss and consequently, the signal produced by a MIP will be proportional to the average of the collection efficiency along its trajectory. An example of these “average” collection efficiency distribution along a row (which in our case is the border of our sample cross-section at the electrodes) is given in Fig.19, both for a non-irradiated and for an irradiated case. The “columns” correspond to y-coordinates in Fig.11 and 12 and divide a total width of 450 μm in 128 bins, displaying therefore each bin a “width” of about 3.6 μm . For such a thin bin width, fluctuations of signal or efficiency are clearly important, even in the irradiated case. It is easy to observe that there is a certain correspondence in fluctuations between the irradiated and the not irradiated case and that the increase in collection efficiency is roughly, but not always, constant. It must be taken into account, also, that statistics are relatively poor, because we wanted to avoid any possible kind of priming effect during the measurement itself and as a consequence, some of the fluctuations could be statistical in nature. By this average procedure, necessary to simulate MIPs, it can be observed that the detector becomes, obviously, more homogeneous, as it is proved in Fig.20, where the distribution of collection efficiency among the various “columns” or possible MIPs trajectories is reported, both for the irradiated and not irradiated case. From this point of view, the main effect of priming is the increase of the average collection efficiency (even in this case by a factor of about 1.8), while the improvement of the homogeneity is less observable. However, it must be noticed that the “energy resolution” (as usually defined) improves from the non-irradiated to the irradiated case, i.e. fluctuations are reduced if considered as percentages of the average value. Finally, it must be noted that the curve

for the non-irradiated case is not a line drawn to guide the eyes, but a real fit with two Gaussians fixed at 0.15 and 0.29 and with standard deviations of 0.073 and 0.037 respectively. In the irradiated case, only one Gaussian is enough for the fit, with a central value of 0.29 and a standard deviation of 0.068. Taking into account only the most prominent peaks, the conclusion is that energy resolution improves from 50% in the non-irradiated case to 33% in the irradiated one. It really seems that in the irradiated case the peak with an average value of 0.15 collection efficiency disappears and it is “transferred” to the peak at 0.29. In other words, it could be concluded that priming cancels out the “phase” of moderate collection efficiency in CVD diamond, by “transforming” it into a high collection efficiency “phase” which, at least in a small percentage (20% in this case), is present also in the virgin sample.

9 . Homogeneity of collection and counting efficiencies for MIPs

By grouping now the columns in bins of different sizes, it is possible to obtain the homogeneity of collection and of counting efficiency as a function of the bin size v_j by the following equation

where:

$$v_j = 1 - \frac{\sqrt{\sum_i N_{i,j} (\eta_{i,j} - \langle \eta \rangle)^2} / \sum_i N_{i,j}}{\langle \eta \rangle}$$

- $\langle \eta \rangle$ is the overall average collection efficiency
- $\eta_{i,j}$ is the average collection efficiency of the bin i of bin size indicated by j
- $N_{i,j}$ is the number of bins of the bin size indicated by j which have an average collection efficiency $\eta_{i,j}$

The result of this analysis is shown in Fig.21 both for the non-irradiated and the irradiated case: particularly in the latter case the uniformity is already good just at lower bin sizes, but it does not reach the value of 100% up to a bin size of half of the region width. For a bin size corresponding to the best attainable spatial resolution in strip detectors, however, the maximum uniformity is of the order of 85%. Data reported in Fig.21 qualitatively agree with analogous data experimentally obtained with MIPs [8]. Same conclusions can be drawn with respect to the counts distribution, i.e. the counting efficiency, even if in our case we do not make use of an electronic threshold. In fact, Fig.22, which is analogous to Fig.20, shows the counts distribution as a function of position y along a row in the electrode plane. By the strong shift of collection efficiency occurring in the irradiated case, (see Fig.20), it can be expected that counting fluctuations are drastically reduced in the irradiated case, as clearly shown in this figure. Counting efficiency uniformity behaviour as a function of bin size is shown in Fig.23: while it is very low for the non-irradiated case even up to

very large bin sizes, for the irradiated case it overcomes 90% just at smallest bin sizes. It can be concluded that the improvement of collection efficiency and of its homogeneity due to priming has its major effects in the counting efficiency homogeneity than in the collection efficiency homogeneity, as it can be observed by looking at Figs.21 and 23.

The agreement with data obtained with CVD diamond strip detectors is of course more qualitative than quantitative, not only because the samples are different and in one case the sample is equipped with strip-like electrodes, but also because of the different averaging procedure, which in [8], Fig. 4.66 refer to square bins or in any case to two-dimensional regions and not, as in this case, to linear bins. Moreover, also the definition of uniformity is not the same, because measurements carried out with MIPs include Landau fluctuations and statistical fluctuations are not included in the definition itself. But the comparison can be pushed even further : Fig. 21 (irradiated case) could be for instance compared with Fig. 4.63 of [8], which reports a similar distribution. The SD in our case is about 0.3 which is very close to rms value quoted there (0.31) and reported also in Fig. 4.64. Please note also that in Fig. 20 the increment factor of the average charge collection length during the priming is 1.9, very close to factor 1.8 reported in [7].

10. Results obtained with other samples

As it was noticed, the results reported so far refer to a sample which was only cut on the substrate side and not polished. We can argue that in this case the contacts are not the same, since the growth side is as-grown and not even cutted. It is therefore quite understandable, apart from any kind of model or interpretation, that the behaviour of the electrical field turns out to be asymmetric.

Other results, unfortunately not complete, could be reported in which the contacts behaviour is much more symmetric *because the contacts or the surfaces are prepared in same way.*

Fig. 24 shows the charge collection efficiency profile at +600 V obtained with another sample, 400 μm thick, which was *finely polished on both sides*. The fit was carried out in the same way as in Fig. 2. Collection efficiency is much lower than in the previous case because the thickness is double, but the ratio between the contributions of electrons and holes is always around 10, as before. The fitting procedure, carried out in the same way, leads to the results shown in Fig. 25, which are very similar to those ones reported in Fig. 3. Electric field and collection length peaks at the anode are less pronounced now and, being the sample thicker , i. e. with much less material cut away at the substrate side, $(\mu\tau)$ products at the back is much lower than in Fig. 3, while they are almost the same at the front. Looking now at Fig. 26, which displays a case of -600 V applied to the same sample, it easy to observe that the behaviour is completely different from Fig. 4. The top efficiencies remain the same and a broad band appears at the right. Apart from a large dip at the cathode, the profile is almost spatially reversed with respect to Fig. 24. This conclusion can be even

more appreciated by looking at Fig. 27 : now we have a sharp peak of the electrical field at the right , i. e. always at the anode and ,as a consequence, another sharp peak of the collection length ($\mu\tau$) product behaviour has been kept equal to the positive bias case). The average value of the collection lengths as seen by MIPs for both polarities are always equal (as it can be observed by looking at the areas under the profiles of collection lengths), but this macroscopic observation hides , as for the previous sample, a not uniform profile of the electric field and, as a consequence, a profile of the collection length strongly dominated by the electronic properties of the region close to the growth side. Consider now for a moment the peak values of collection length for electrons : values up to 200 μm (Fig. 27) or up to 600 μm (Fig. 25) or even up to 1.6 mm as in Fig. 3 can be found. Even if a caution word should be spent remembering that we do not prove, but we are considering only compatibility aspects between our and other's results, it is clear that, without knowing exactly the behaviour of contacts (and our contacts should be considered as standard), it is not possible to extrapolate from measurements carried out with minimum ionising particles values of collection length that refer to the bulk of the CVD diamond sample. In fact, also in this case, with respect to the above-mentioned maximum values of collection length, the average or bulk value of collection length is always about 50 μm .

11. Conclusions

We have demonstrated that the linear model is compatible with micro-IBIC data, if as a “linear model” is intended a linear behaviour of $(\mu\tau)$ product from the substrate to the growth side. Because of effects at the electrodes, and particularly at the growth surface, it can be by no means assumed that a linear behaviour of collection length takes place. Charge collection seems to be almost entirely due to electrons.

The electric field profile seems to be dependent on the surface preparation and it is different for polished surfaces with respect to cut ones.

Because of the better transport properties of electrons, collection efficiency profile as a function of depth has a maximum at the cathode (for negative bias applied to the growth side) while it has a broad maximum in the central region for positive bias . As a result of this compensation between the electric field profile and the $(\mu\tau)$ product behaviour, the average collection length as simulated along the thickness of the sample has the same values both for positive and negative bias voltages, a result which was previously found by direct measurements with α -particles as reported in **Errore.**

L'origine riferimento non è stata trovata.. The effect of priming is essentially an almost uniform increase of collection efficiency for MIPs, and a reduction of fluctuations, as indicated microscopically by a much more homogeneous behaviour of the detector.

The simulation of the behaviour of MIPs by using the results of IBIC measurements finally leads to

a qualitative agreement with experimental data as far as the homogeneity of both the collection efficiency (or MIPs signal) and the counting efficiency are concerned.

In conclusion, the linear model, in a version referring to $(\mu\tau)$ product instead of collection length, has been proved to be compatible finally both with IBIC results and with data obtained by MIPs. A linear model referred to collection length could be valid only if contacts related problems will be solved. However, the contacts problems seem to be somehow related to the particular nature of CVD diamond

References

- [1] C.Manfredotti, F.Fizzotti, P.Polesello, E.Vittone, P.Rossi, G.Egeni, V.Rudello, I.Bogdanovic, M.Jaksic and V.Valkovic, “*Proton microbeam investigations on electrical properties of natural and CVD diamond*”, Nucl. Instr. Meth. in Phys. Res., B130 (1997) 491
- [2] C.Manfredotti, F.Fizzotti, E.Vittone, M.Boero, P.Polesello, S.Galassini, M.Jaksic, S.Fazinic, I.Bogdanovic “*IBIC investigations on CVD diamond*”, Nucl. Instr. Meth. In Phys. Res., B100, (1995) 133
- [3] M.Mishina “*Signal Formation in Diamond Detector*” (Feb.1999) RD-42 Meeting minutes, LETI, Saclay (France)
- [4] J.S.Conway et al. “*RD-42 Test Beam Analysis*” (Oct. 1997), RD-42 Meeting minutes, Toronto (Canada)
- [5] C.Manfredotti, F.Fizzotti, P.Polesello, P.P.Trapani, E.Vittone, M.Jaksic, S.Fazinic and I.Bogdanovic, “*Investigation on the electric field profile in CdTe by ion beam induced current*”, Nucl. Inst. Meth. In Phys. Res., A380 (1996) 136
- [6] C.Manfredotti, Fizzotti and E.Vittone “*IBIC investigations of radiation-induced effects in CVD and natural diamond*” Nucl. Instr. Meth. in Phys. Res. A426 (1999) 156
- [7] See for instance D.Meier, “CVD Diamond Sensors for Particle Detection and Tracking”
- [8] Inaugural dissertation, Dusseldorf 1999, p. 93
- [9] C. Manfredotti, F. Fizzotti, M. Boero, E. Vittone and P. Polesello, “ *Characterization of CVD diamond films by nuclear techniques with α particles* “, Diamond and Related Materials 4 (1995) 517

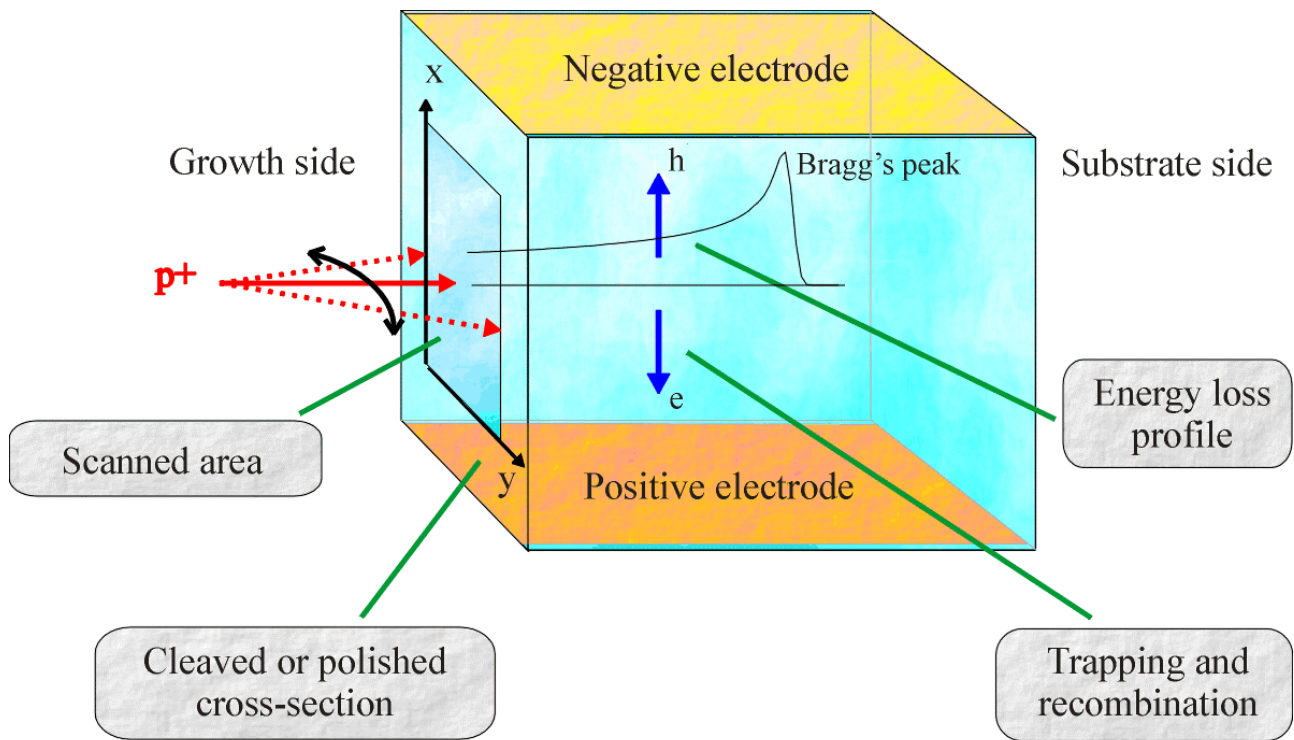


FIG. 1

Fig. 1 – Description of the geometry of irradiation and signal collection in lateral IBIC measurements.

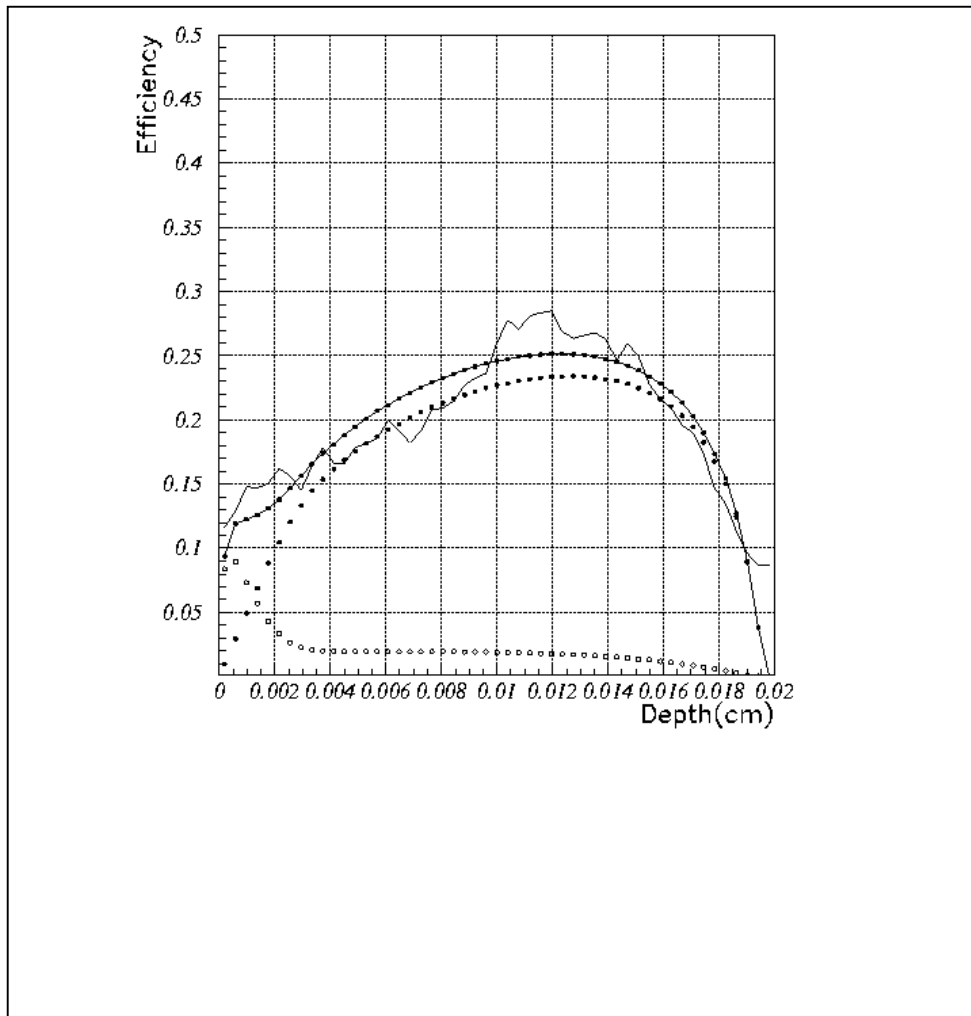


Fig. 2 – Charge collection efficiency profile as a function of depth for a bias voltage of + 400 V applied at the growth side (the left of the figure). The profile has been obtained by an average over a region 450 μm wide. Continuous line : experimental curve. Full dots with a line : fitting curve (see text for details). Full dots and open dots: electron and hole contribution to the collection efficiency, respectively.

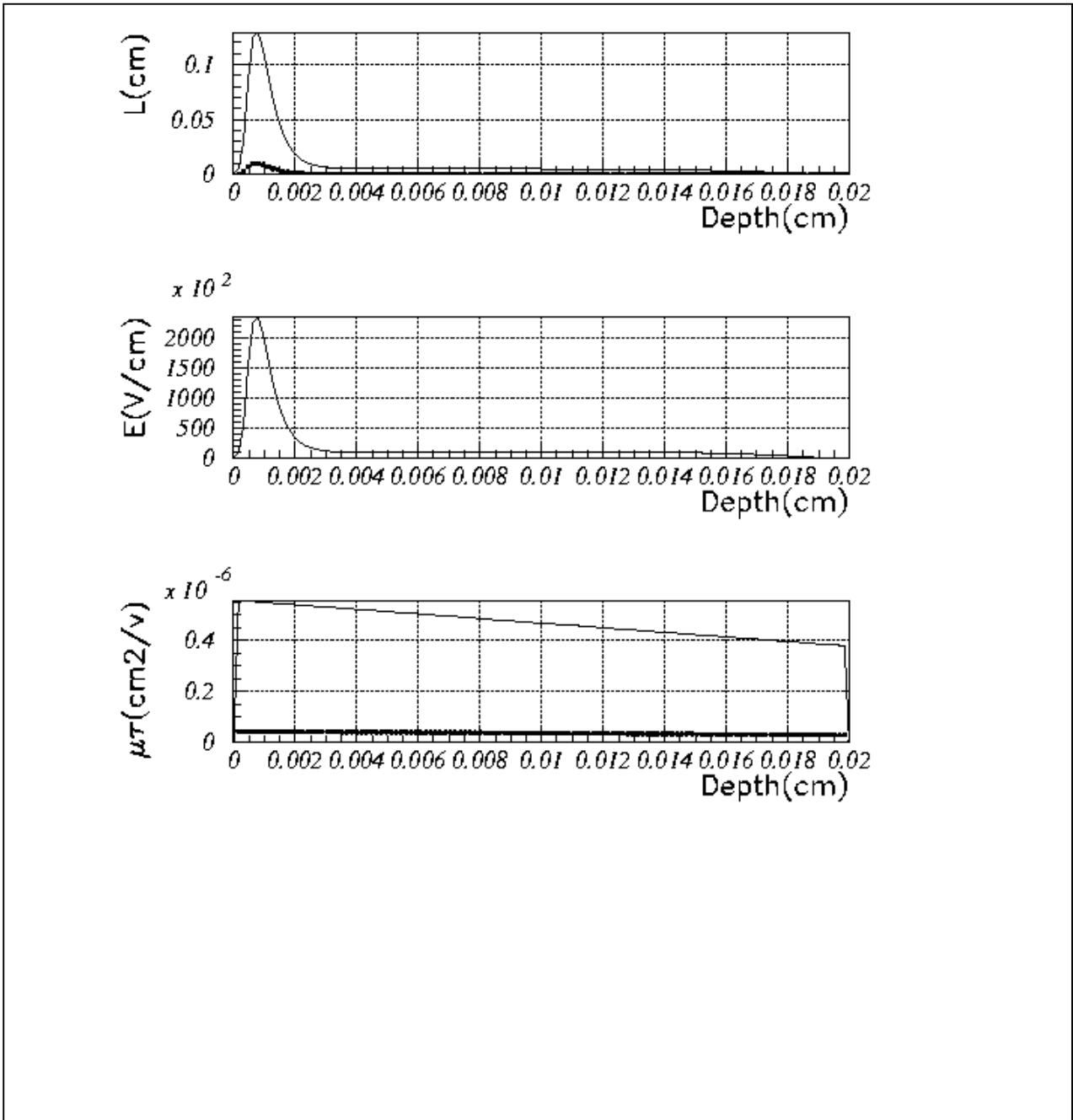


Fig. 3 – Results from the fit applied to data of Fig. 2:

Top : collection length profile for electrons (continuous line) and holes (dots).

Centre : electric field profile

Bottom : (mobility)x(lifetime) profile for electrons (continuous line) and holes (dots)

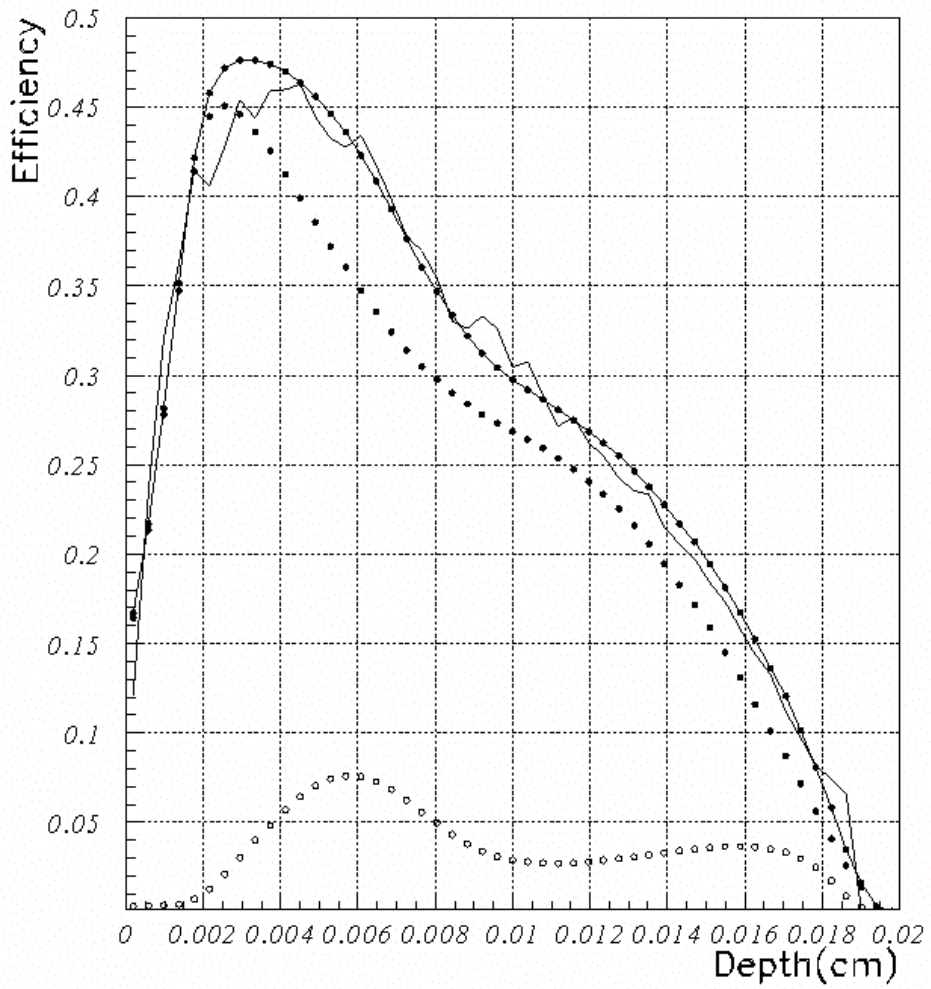


Fig. 4 – Charge collection efficiency profile as a function of depth, as in Fig. 2, for a bias voltage of – 400 V.

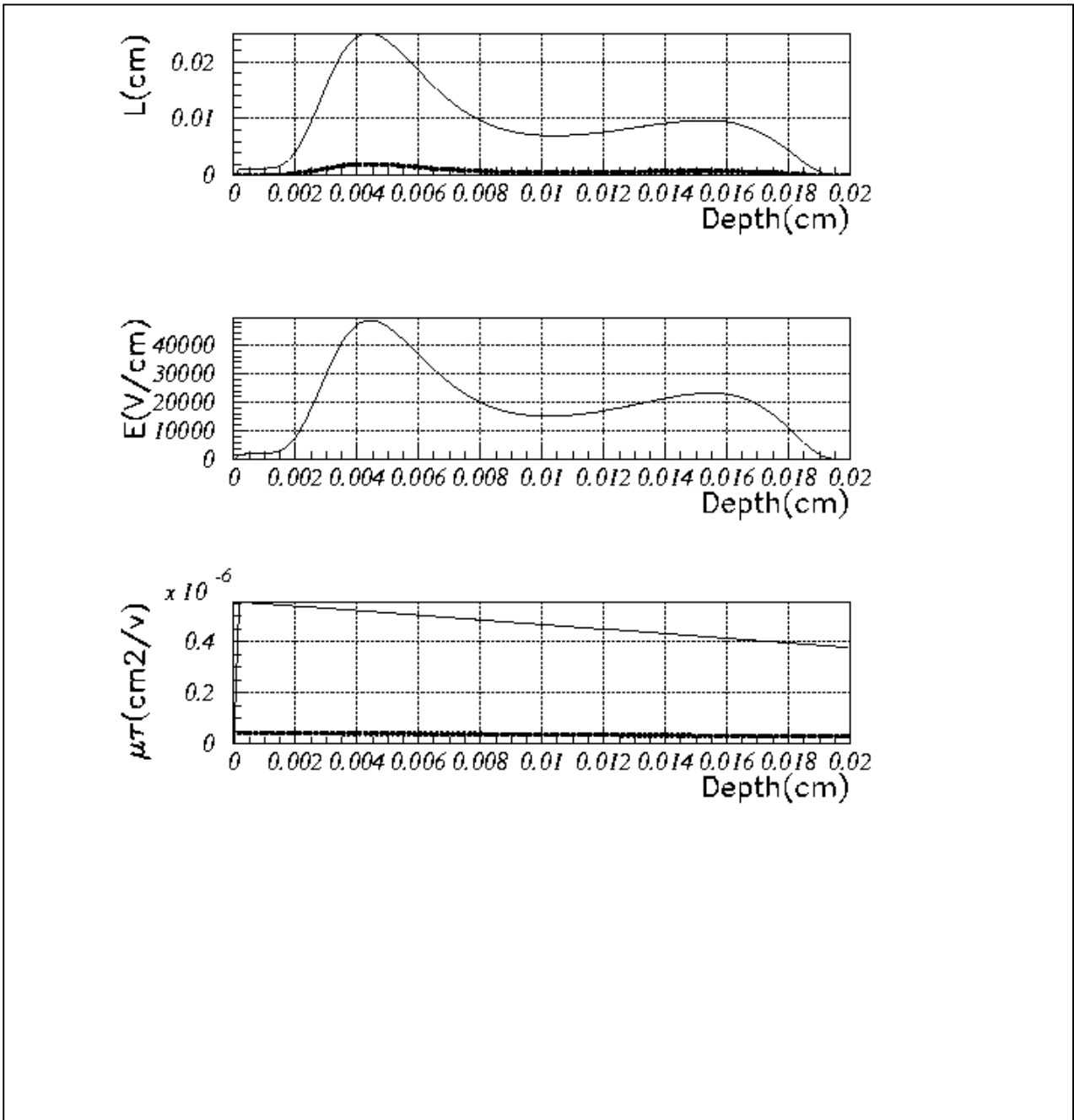


Fig. 5 – Results from the fit applied to data of Fig. 4 (to be compared with Fig. 3) :

Top : collection length profile for electrons (continuous line) and holes (dots).

Centre: electric field profile. Bottom : (mobility)x(lifetime) profile for electrons (continuous line) and holes (dots)

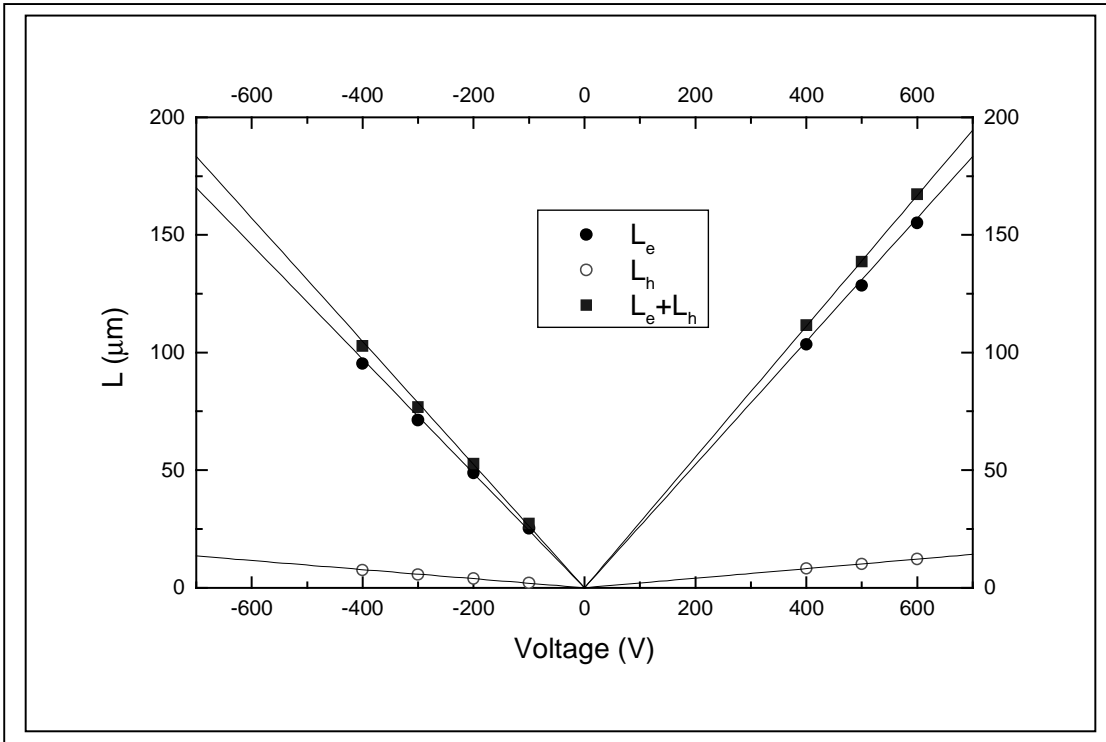


Fig. 6 – Behaviour of mean collection length for electrons (\bullet), holes (\circ) and of both carriers (\blacksquare) as a function of bias voltage. The fitting straight lines crossing the origin indicate mean collection lengths for electrons and holes are strongly linear with bias voltages.

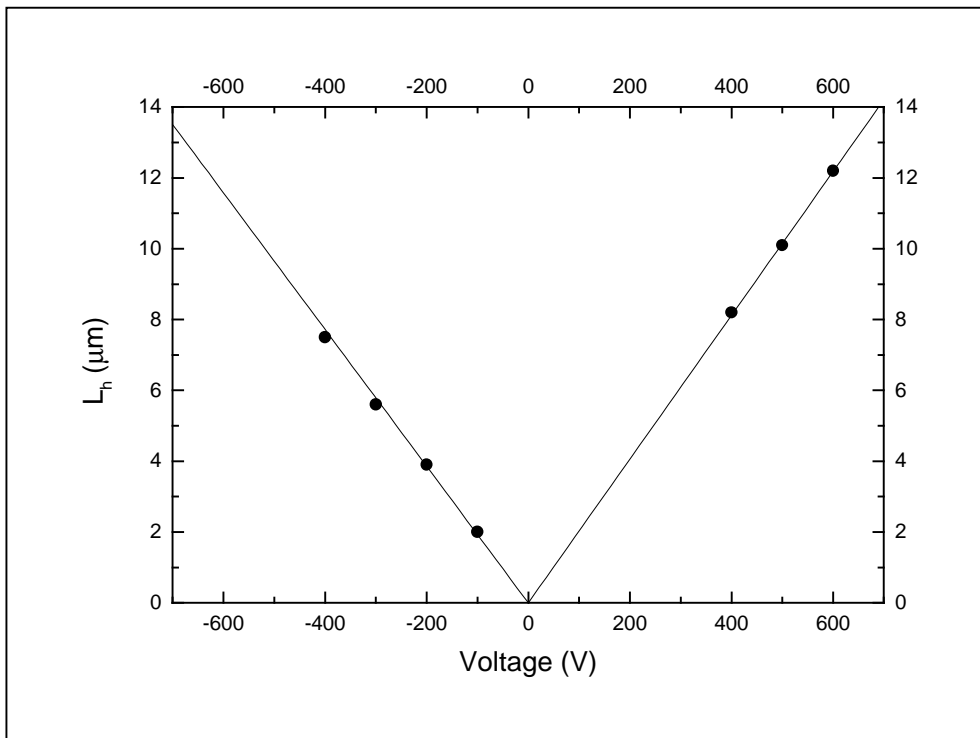


Fig. 7 – Blow-up of holes' mean collection length behaviour at different bias voltages

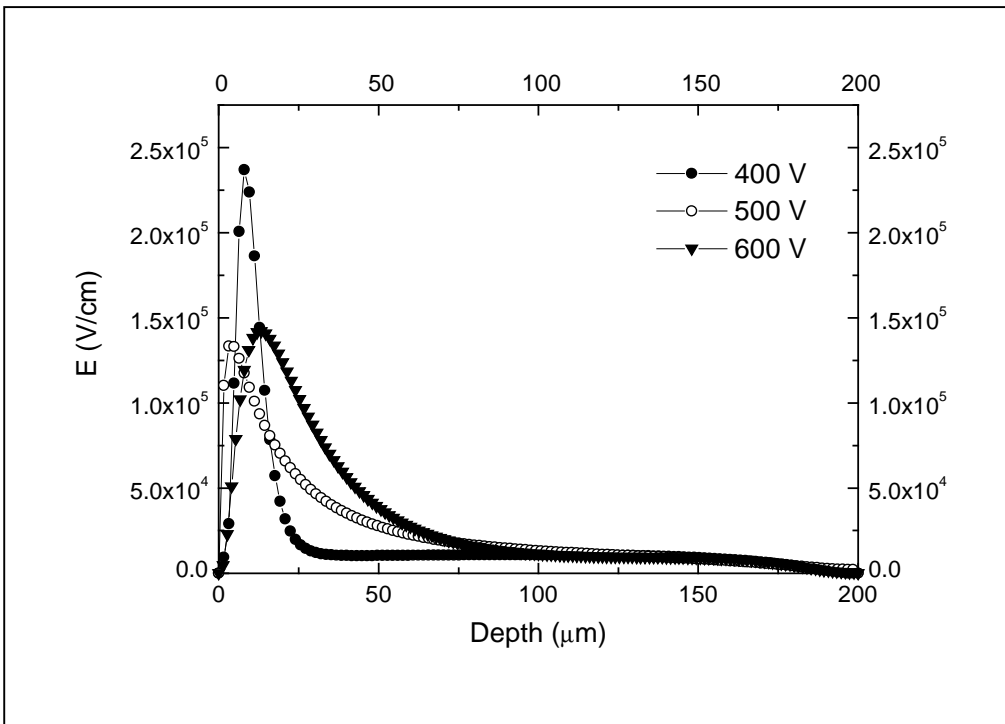


Fig. 8 – Electric field profiles at different positive bias voltages.

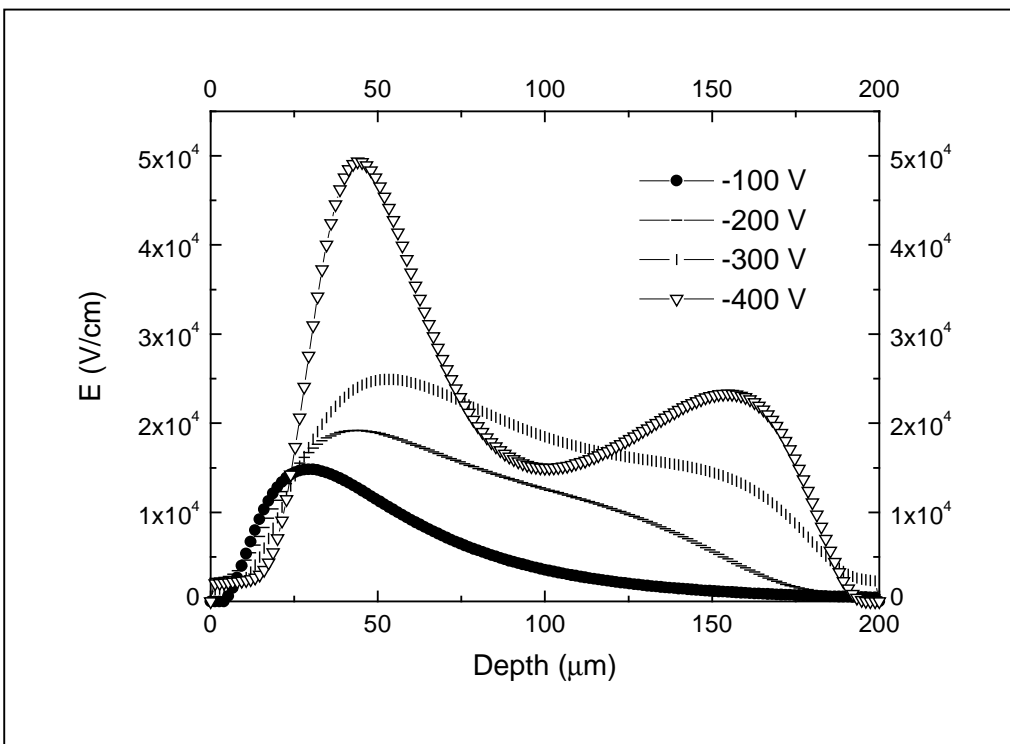


Fig. 9 – Electric field profiles at different negative bias voltages.

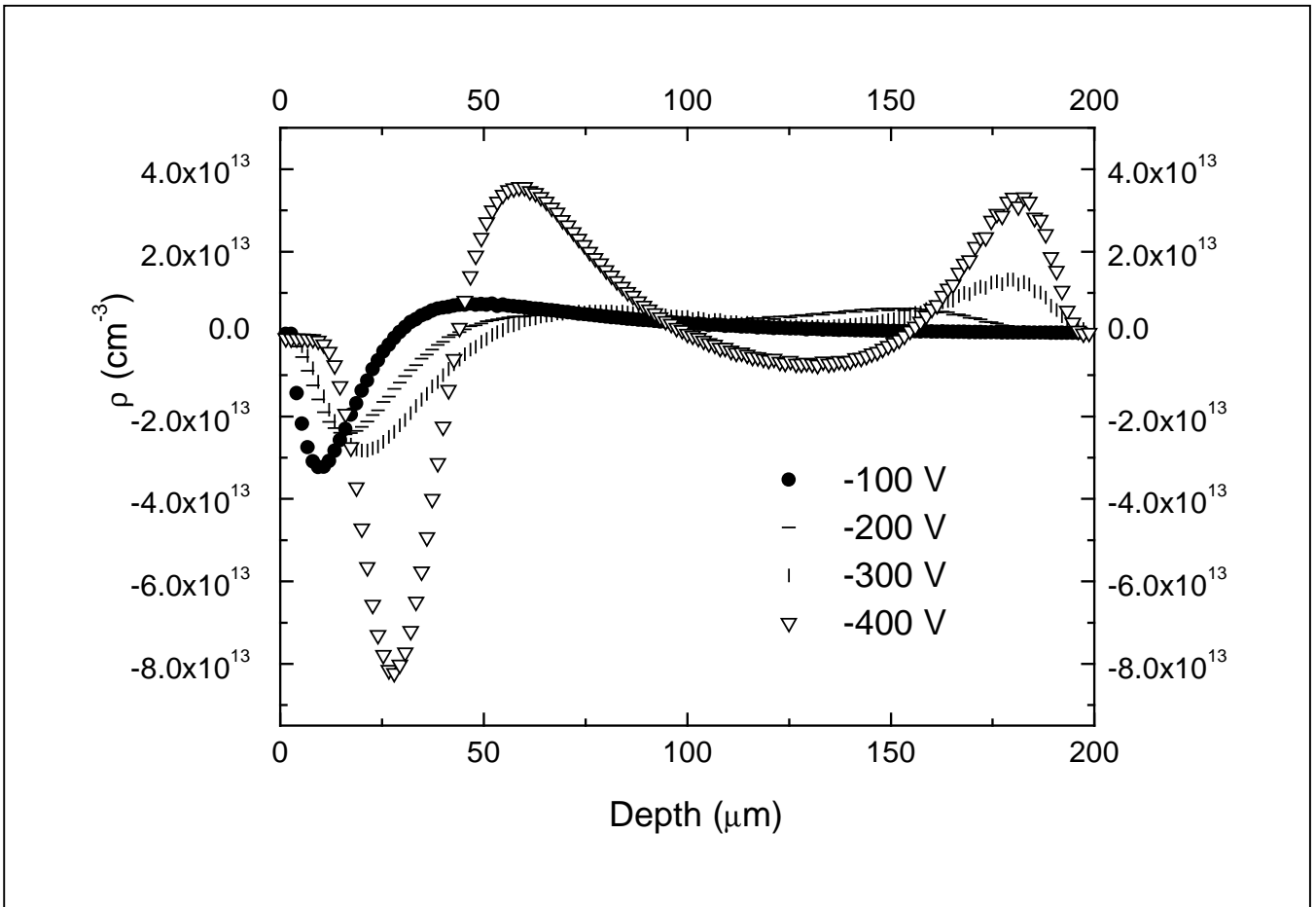


Fig. 10 – Fixed charge density profiles (in electron charge units) at different bias voltages as obtained by differentiating the electric field profiles shown in Fig. 9.

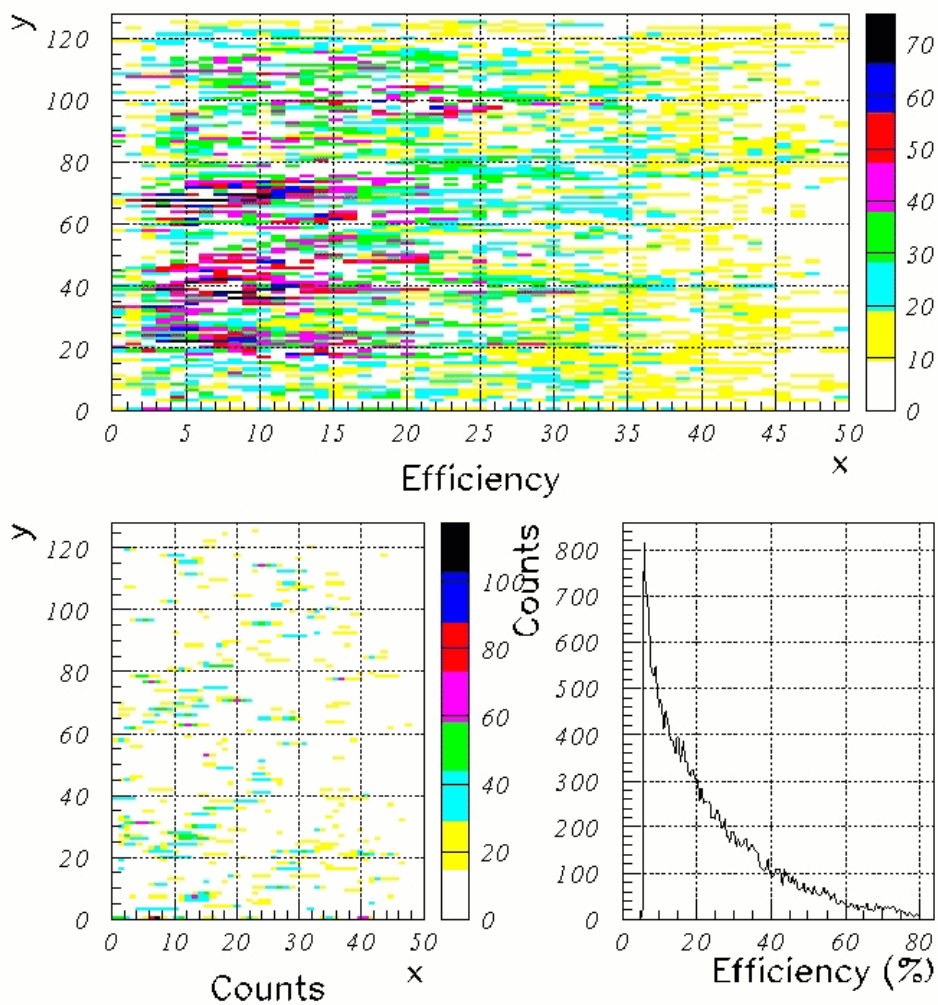


Fig. 11 – Top : Charge collection efficiency map of another cross-section region $450\ \mu\text{m}$ wide (y) of the same sample ($200\ \mu\text{m}$ thick along x). A bias voltage of $-300\ \text{V}$ is applied at the growth side (on the left). Centre : counting efficiency map for the same region. Bottom : pulse height multichannel spectrum relevant to the same region

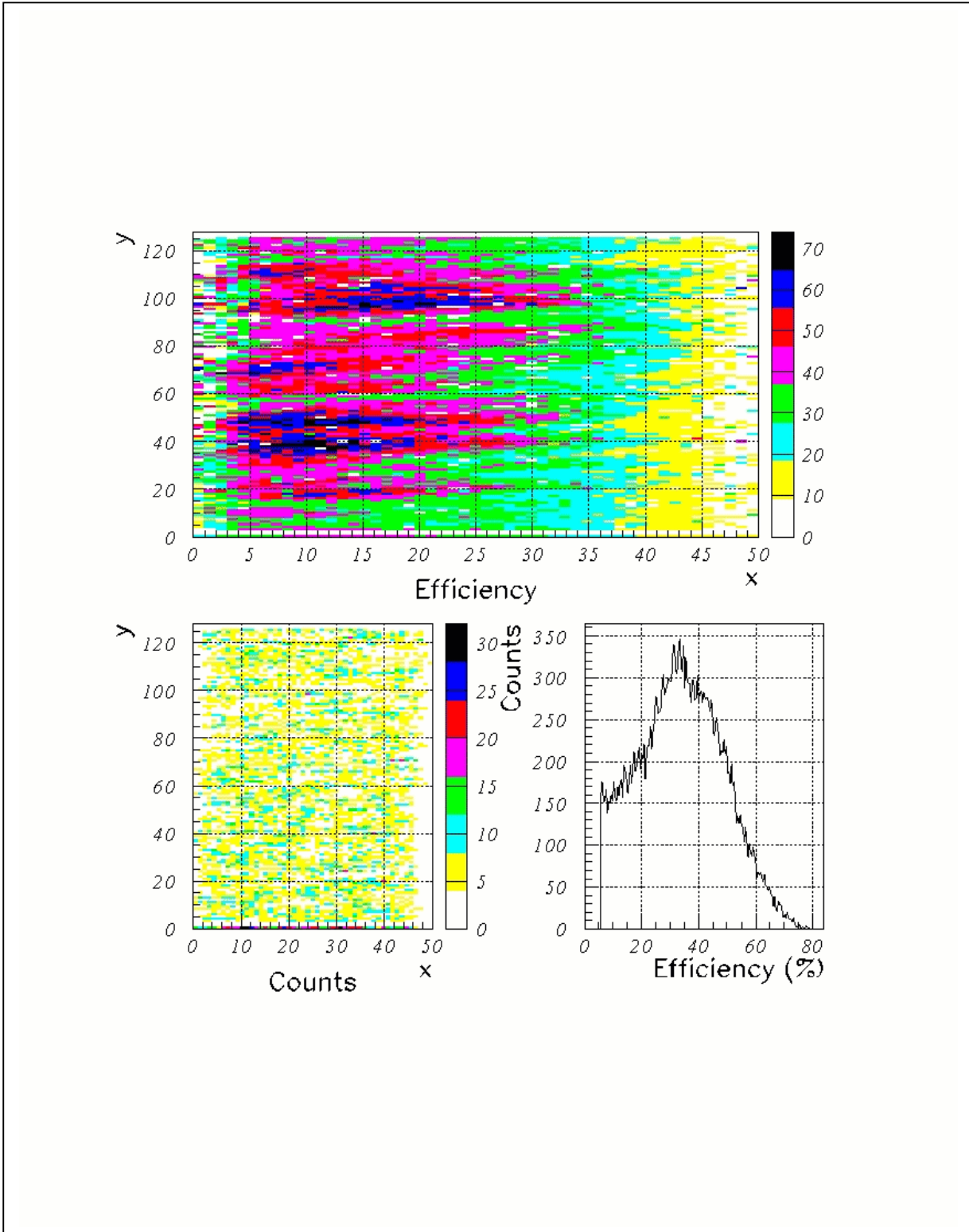


Fig. 12 – Maps and profiles in the same region as in Fig. 11, after an irradiation dose of 46 Gy:
 Top: Charge collection efficiency map of another cross-section region 450 μm wide (y) of the same sample (200 μm thick along x). Growth side is on the left. Centre : counting efficiency map for the same region. Bottom : pulse height multichannel spectrum relevant to the same region

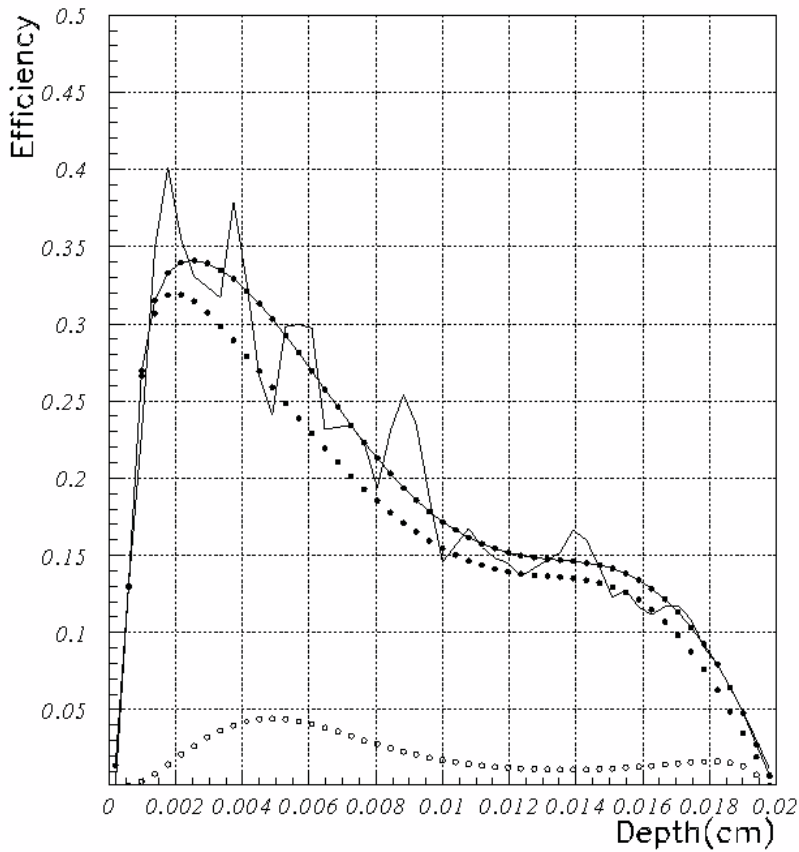


Fig. 13 – Charge collection efficiency profile as a function of depth for a bias voltage of - 300 V applied at the growth side (the left of the figure). The profile has been obtained from the map of Fig. 11 by an average over a region 450 μm wide. Continuous line : experimental curve. Full dots with a line : fitting curve (see text for details). Full dots and open dots : electron and hole contribution to the collection efficiency respectively.

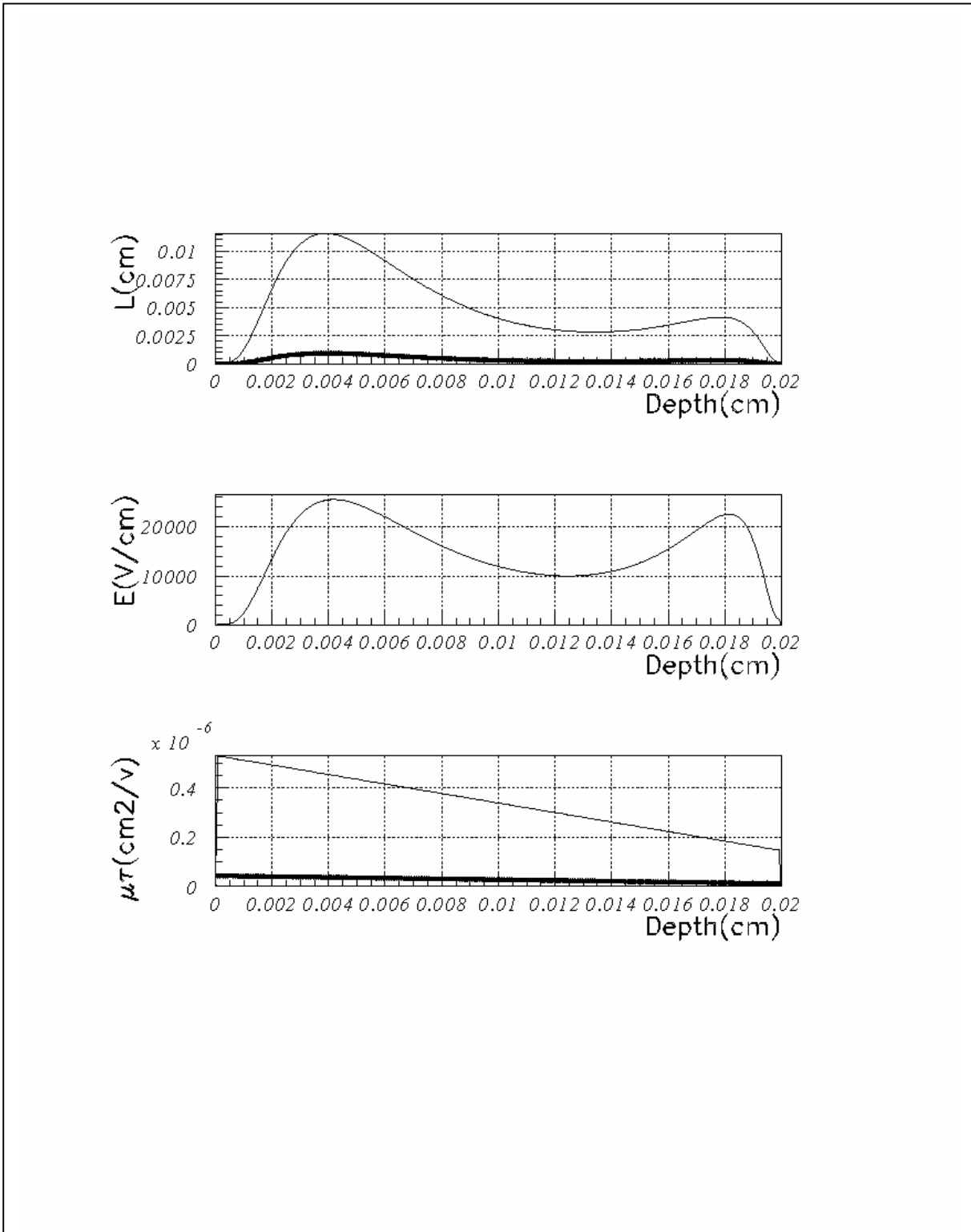


Fig. 14 – Results from the fit applied to data of Fig. 13 (not irradiated case):

Top : collection length profile for electrons (continuous line) and holes (open dots).

Centre : electric field profile. Bottom : (mobility)x(lifetime) profile for electrons (continuous line) and holes (open dots). The mean collection length (over the sample thickness) is 51.1 μm for electrons and 4.2 μm for holes respectively.

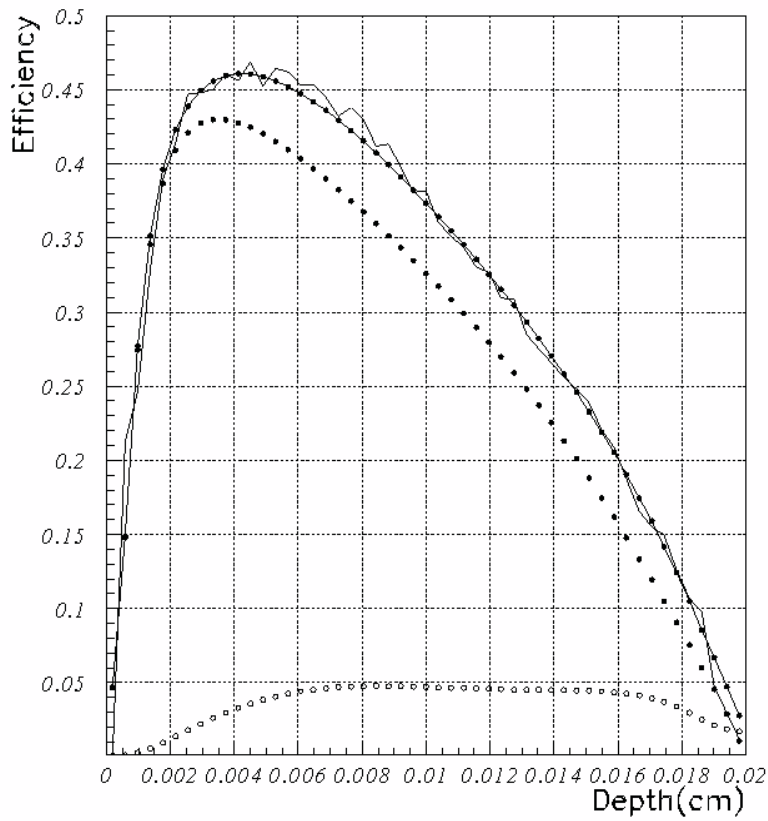


Fig. 15 – Charge collection efficiency profile - in the case of irradiation - as a function of depth for a bias voltage of - 300 V applied at the growth side (the left of the figure). The profile has been obtained from the map of Fig. 12 by an average over a region 450 μm wide. Continuous line : experimental curve. Full dots with a line : fitting curve (see text for details). Full dots and open dots : electron and hole contribution to the collection efficiency respectively. The sample has been irradiated by a dose of 46 Gy.

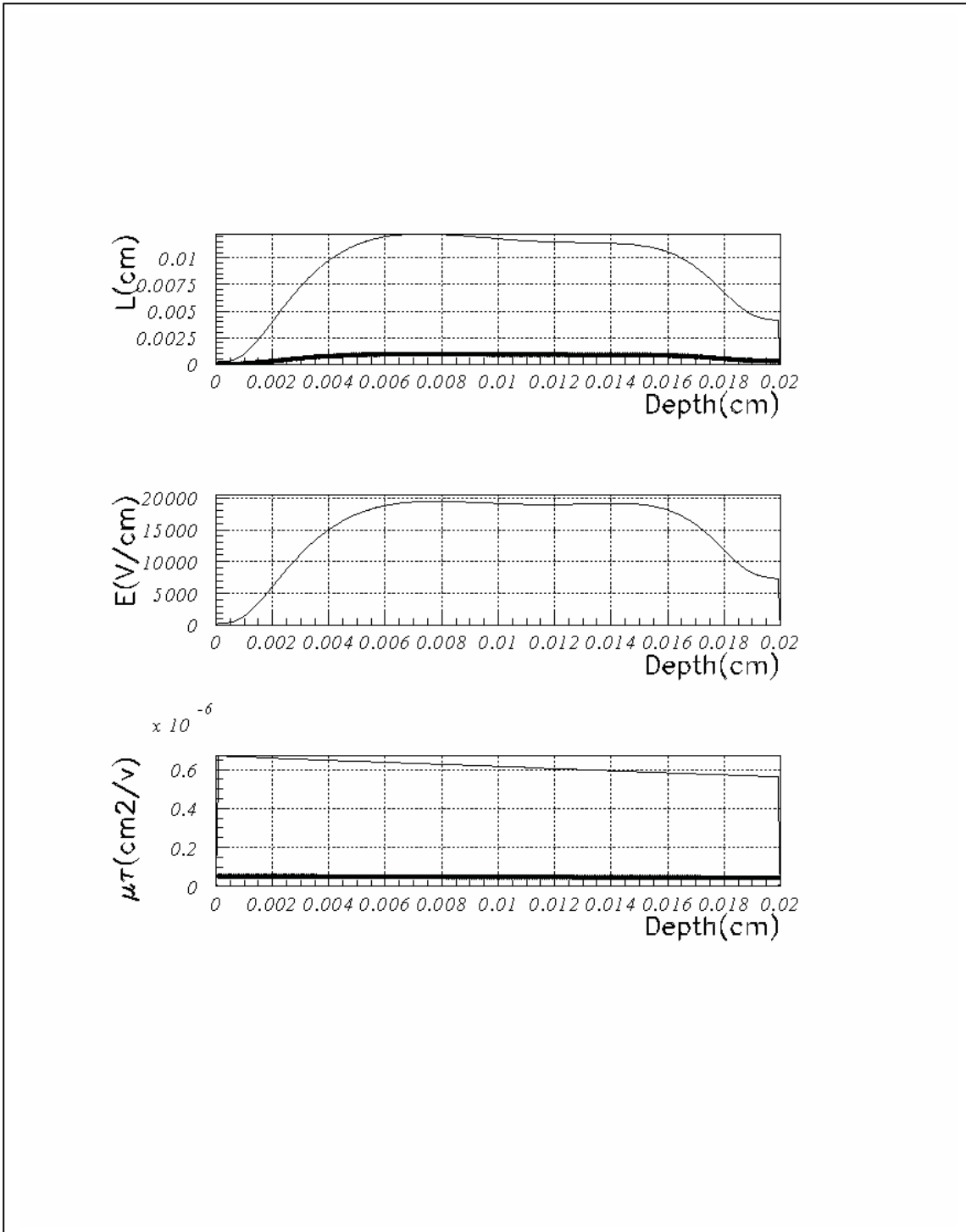


Fig. 15 – Results from the fit applied to data of Fig. 14 (irradiated case): Top : collection length profile for electrons (continuous line) and holes (open dots). Centre : electric field profile
 Bottom : (mobility)x(lifetime) profile for electrons (continuous line) and holes (open dots)
 The mean collection length (over the sample thickness) is in this case 93.2 μm for electrons and 7.7 μm for holes respectively.

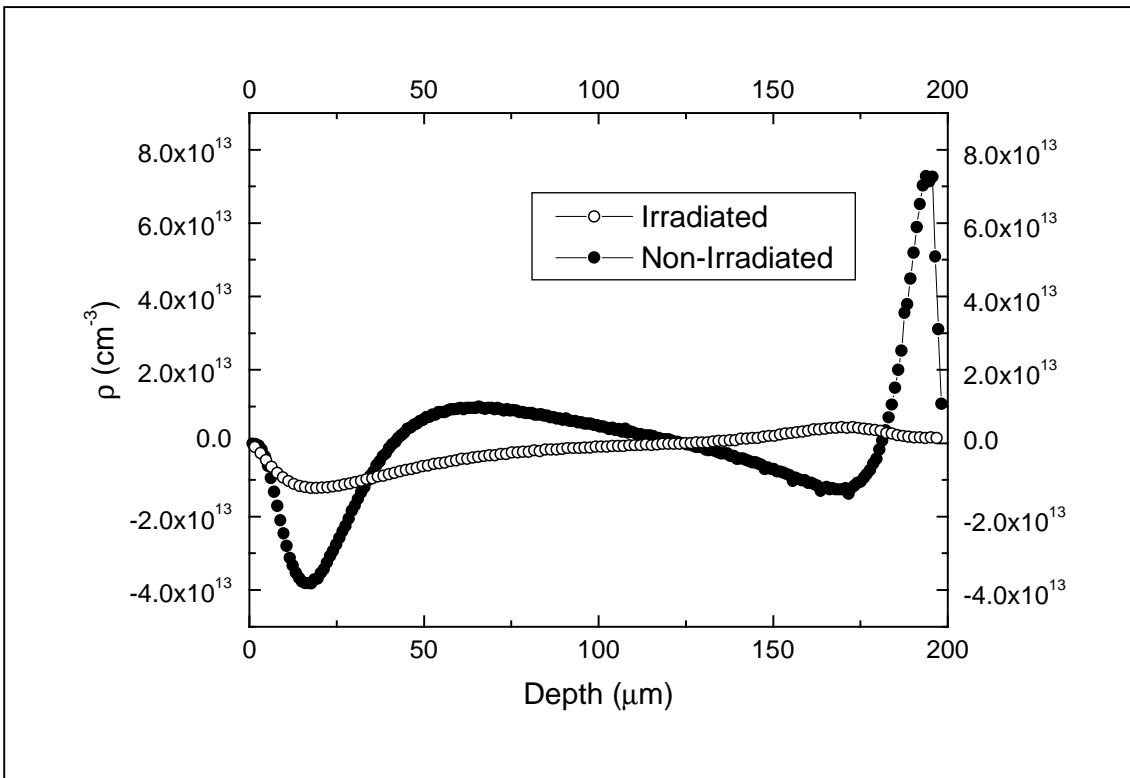


Fig. 17 – Fixed charge density profiles (in electron charge units) at a bias voltage of – 300 V in the cases of no irradiation and of irradiation (or priming), as obtained by differentiating the electric field profiles shown in Figs. 13 and 15 respectively.

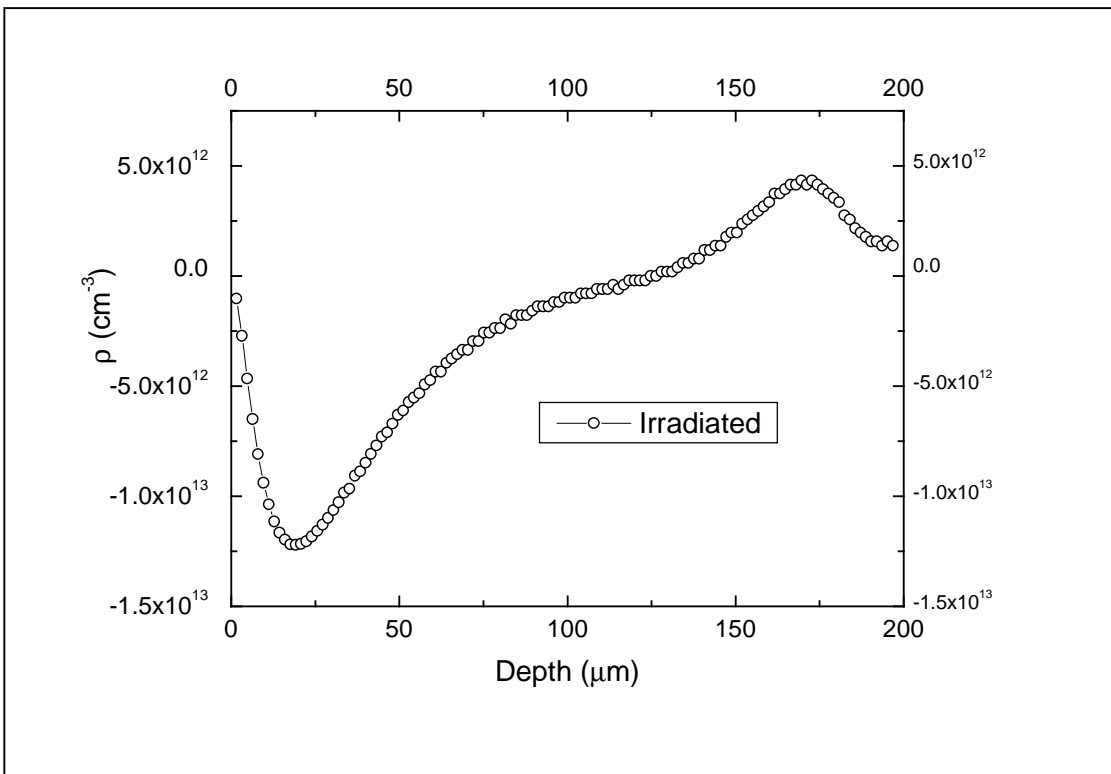


Fig. 18 – Blow-up of Fig. 17 (irradiated case)

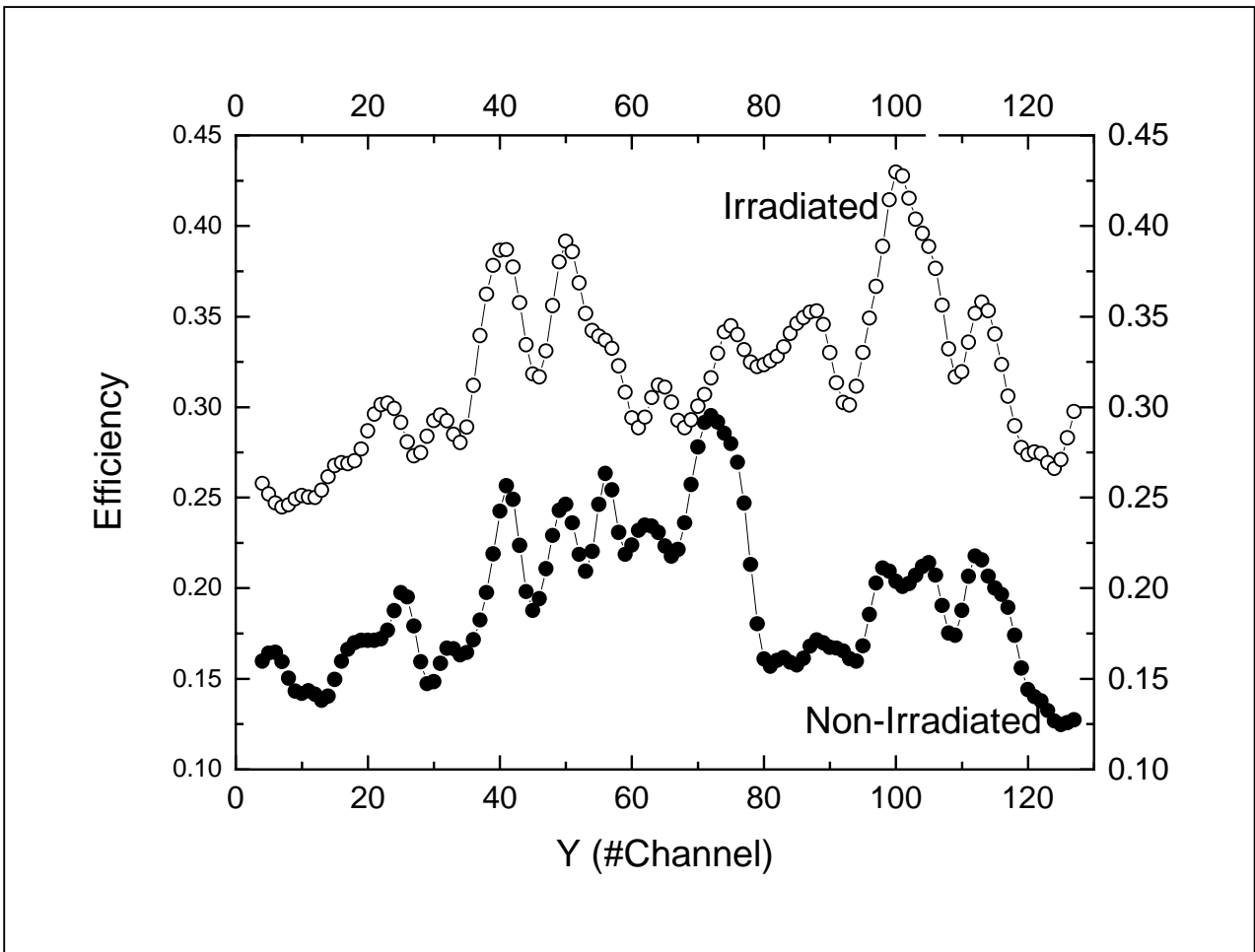


Fig. 19 – Charge collection efficiency profiles along the border of the top electrode calculated by simulating hitting MIPs and by averaging the collection efficiency along the depth of the sample (refer to Figs. 10 and 11 , top maps : profiles are calculated along y direction and averages along x or depth direction) for the irradiated and not irradiated cases respectively.

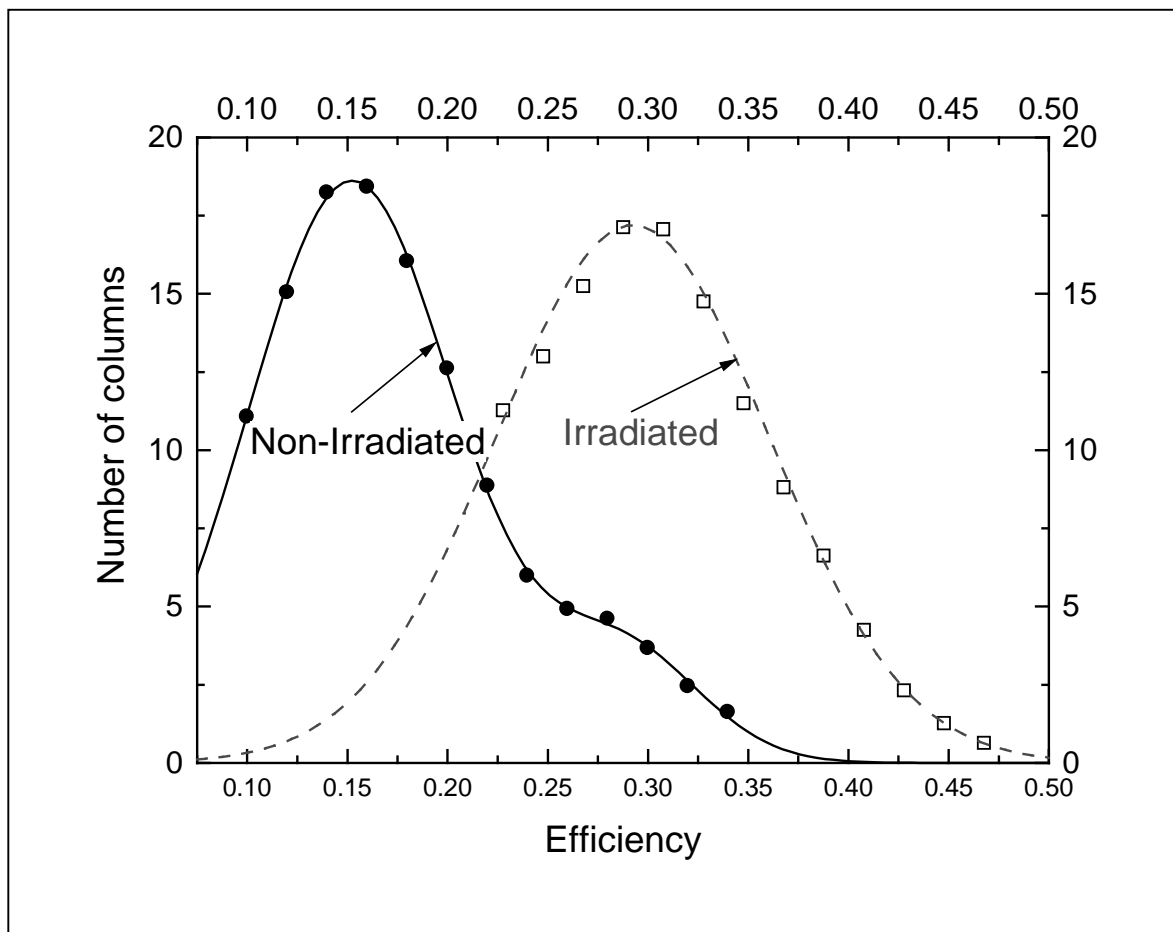


Fig. 20 – Efficiency distribution among the various y positions (defined here as “ columns ”) in the non-irradiated and irradiated case respectively. The continuous line is a fitting line for non-irradiated sample with two Gaussian curves (mean 0.1523 and 0.205, standard deviation 0.073 and 0.037, respectively). The dashed line is a fitting Gaussian curve with mean 0.29 and standard deviation 0.068 for irradiated sample.

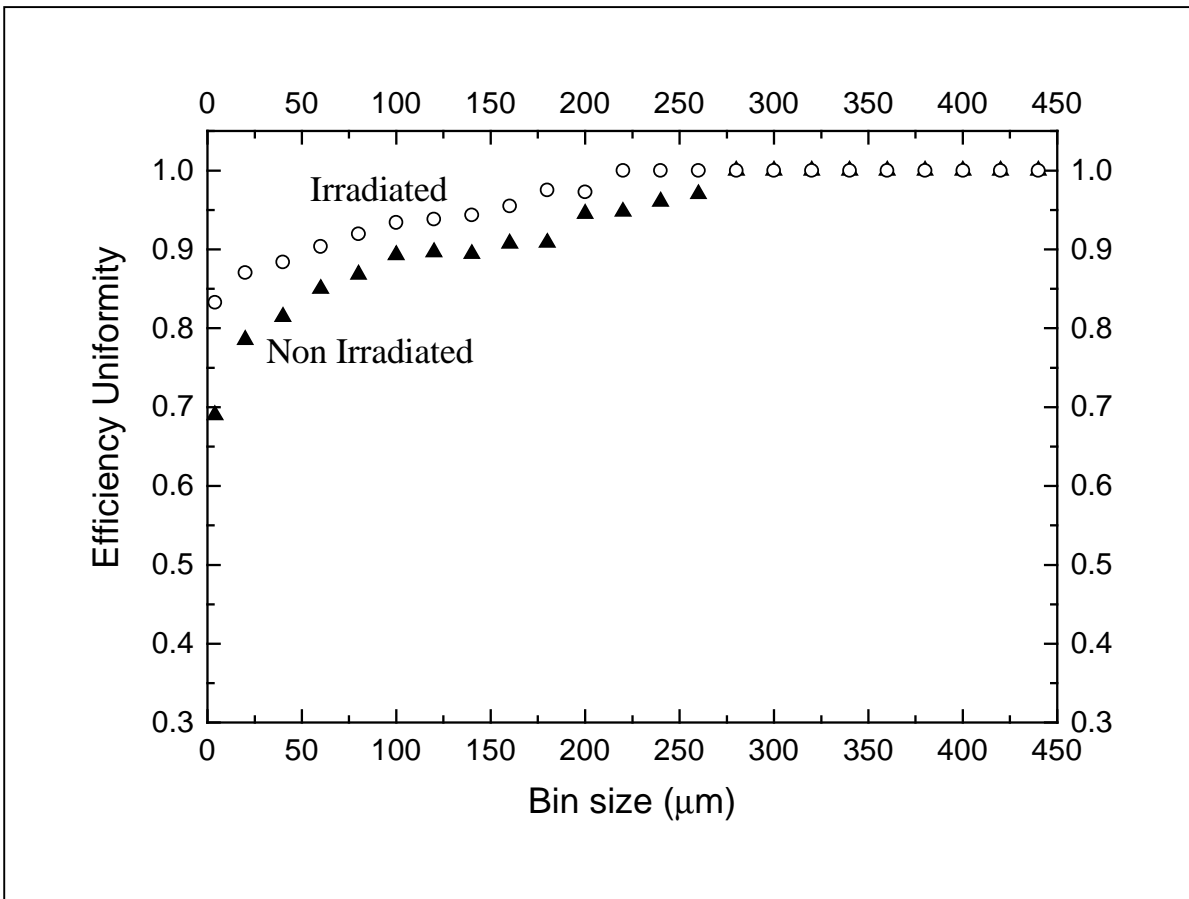


Fig.21 – Behaviour of efficiency uniformity at different bin size for non-irradiated sample (η) and

irradiated sample (η_i). Efficiency uniformity is defined as $1 - \frac{1}{\langle \eta \rangle} \cdot \sqrt{\frac{\sum N_i (\eta_i - \langle \eta \rangle)^2}{\sum N_i}}$, where

N_i is the number of columns having a certain collection efficiency η_i , and $\langle \eta \rangle = \frac{\sum N_i \eta_i}{\sum N_i}$ is the average collection efficiency

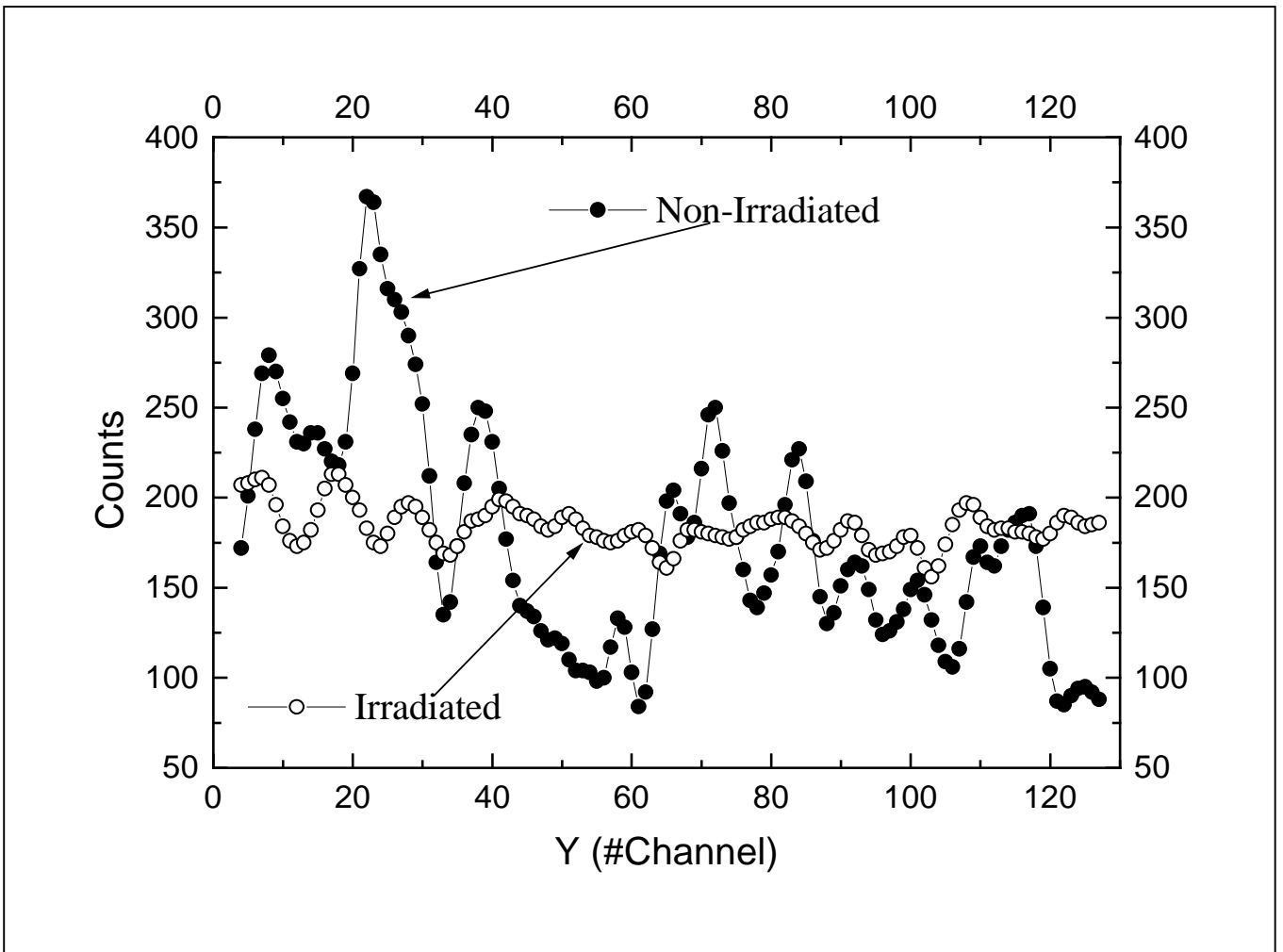


Fig.22 – Counts profiles along the border of the top electrode: solid circles are for non-irradiated case and open circles for irradiated case respectively.

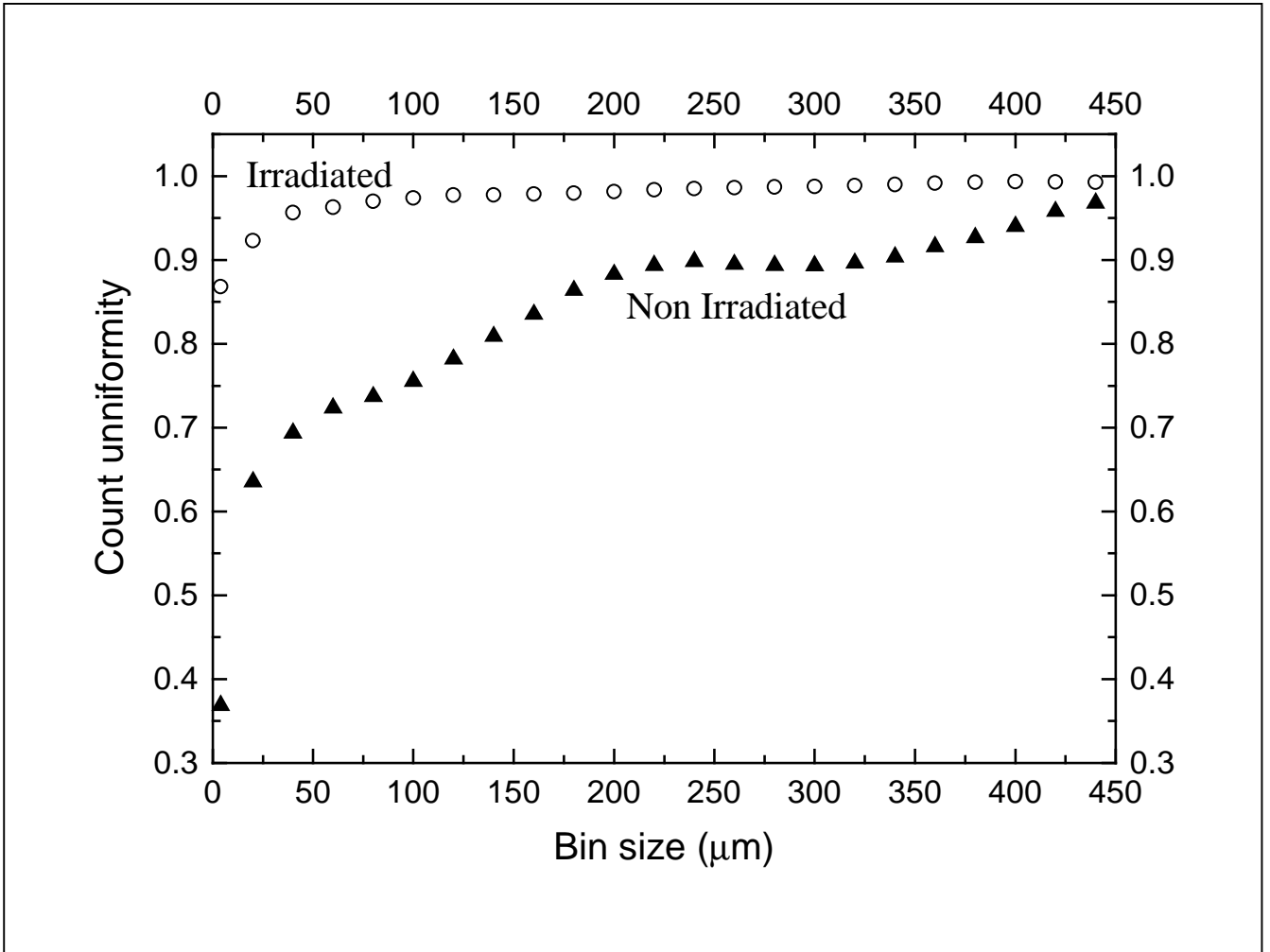


Fig.23 – Behaviour of count uniformity at different bin sizes for non-irradiated sample (▲) and

irradiated sample (○). Count uniformity is defined as $1 - \frac{1}{\langle C \rangle} \sqrt{\frac{\sum N_i (c_i - \langle C \rangle)^2}{\sum N_i}}$, where N_i is

the number of columns having an amount of counts C_i and $\langle C \rangle = \frac{\sum N_i C_i}{\sum N_i}$ is the average amount of counts.

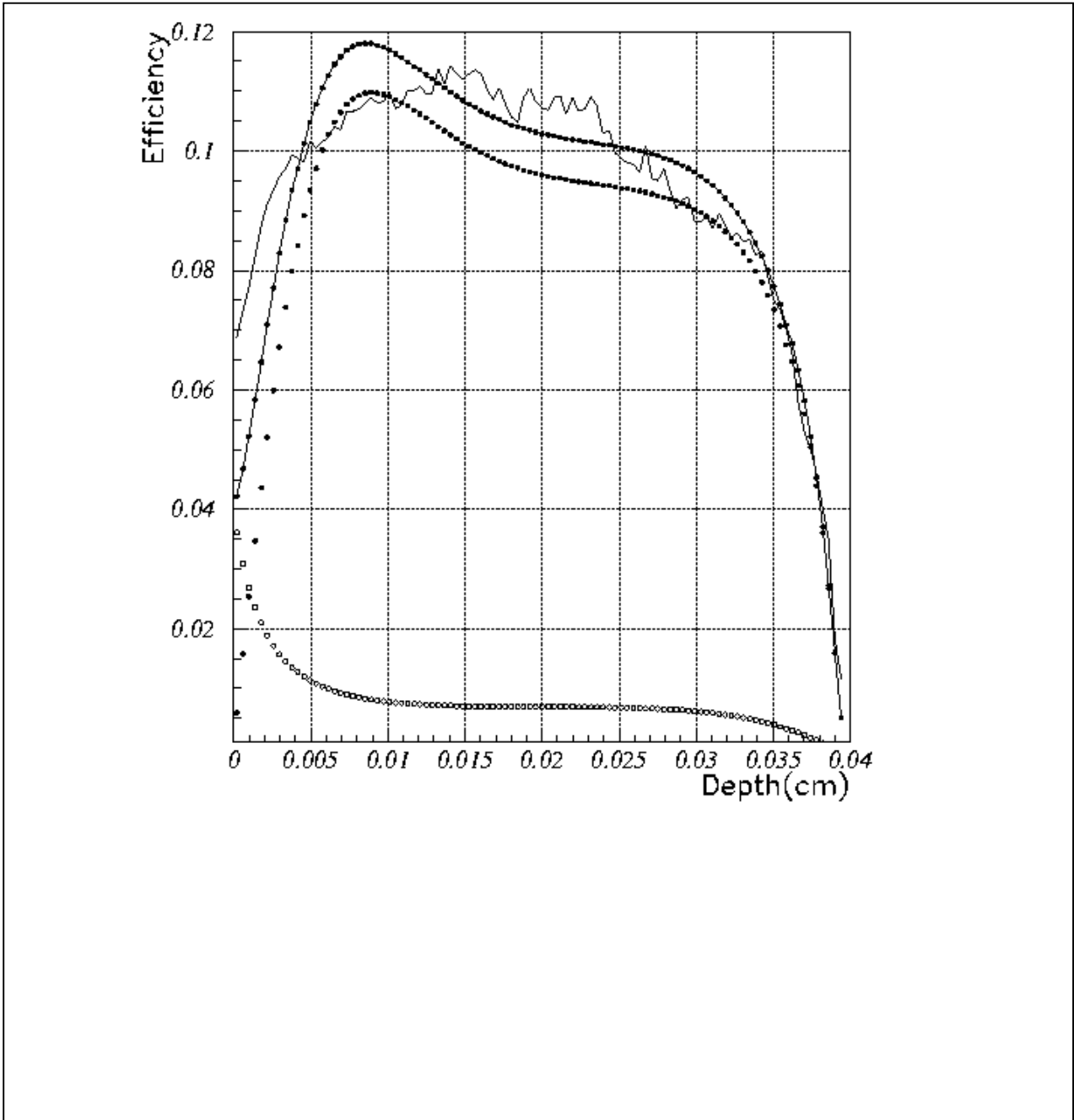


Fig. 24 – Charge collection efficiency profile as a function of depth for a bias voltage of + 600 V applied at the growth side (the left of the figure). The profile has been obtained by an average over a region 450 μm wide. Continuous line : experimental curve. Full dots with a line : fitting curve (see text for details). Full dots and open dots: electron and hole contribution to the collection efficiency respectively.

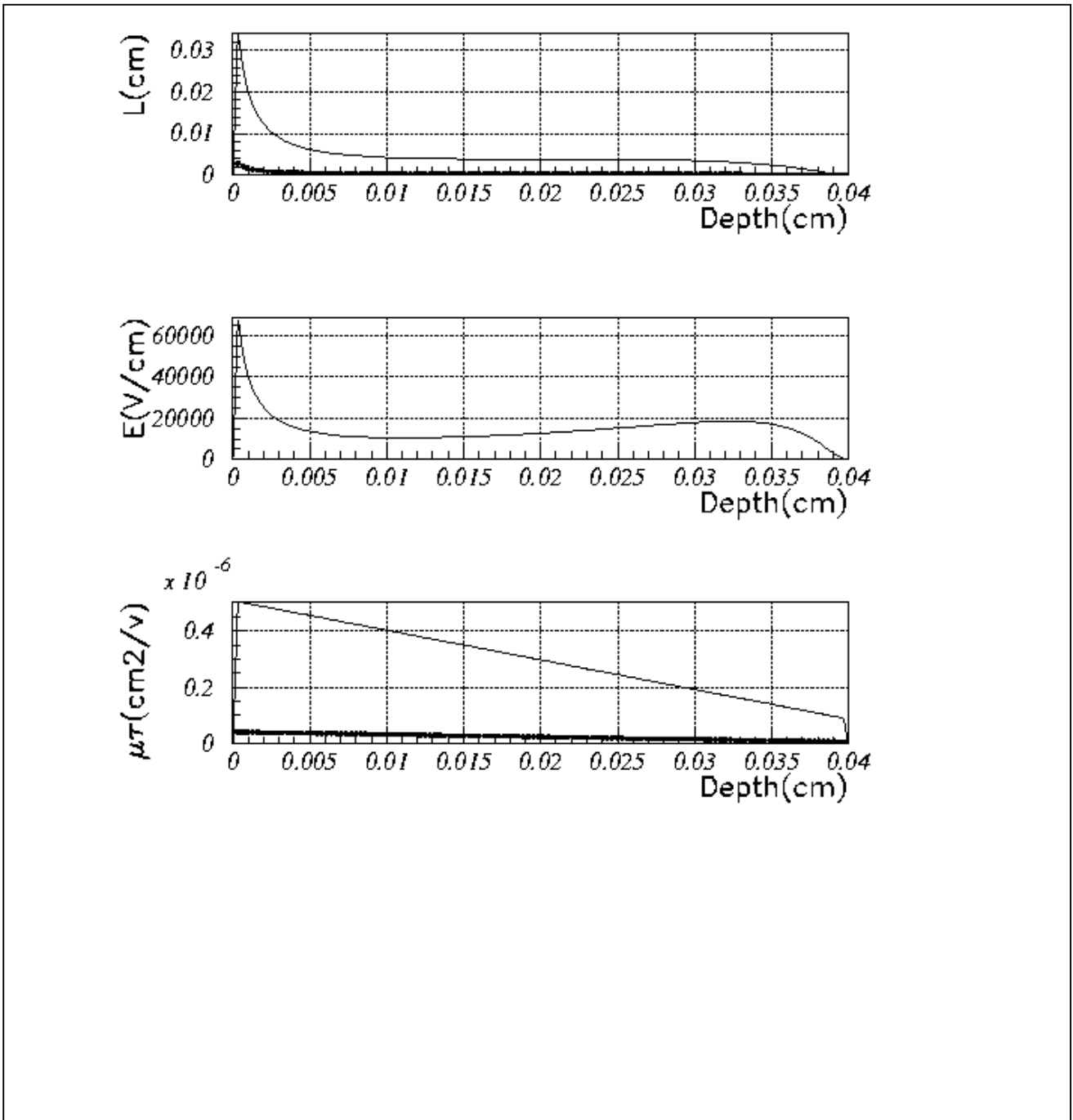


Fig. 25 – Results from the fit applied to data of Fig. 24:

Top : collection length profile for electrons (continuous line) and holes (open dots).

Centre : electric field profile

Bottom : (mobility)x(lifetime) profile for electrons (continuous line) and holes (open dots)

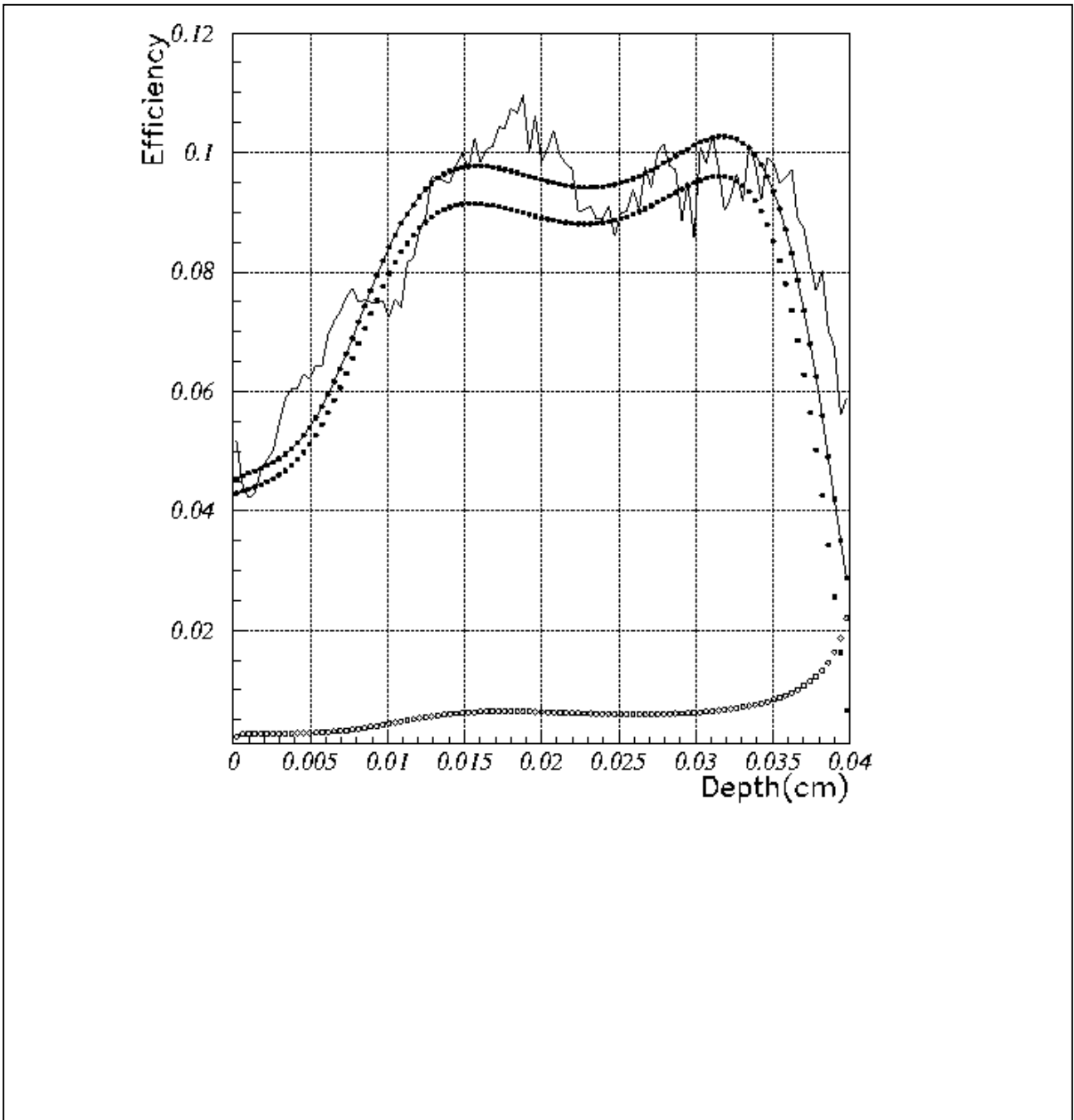


Fig. 26 – Charge collection efficiency profile as a function of depth, as in Fig. 24, for a bias voltage of -600 V.

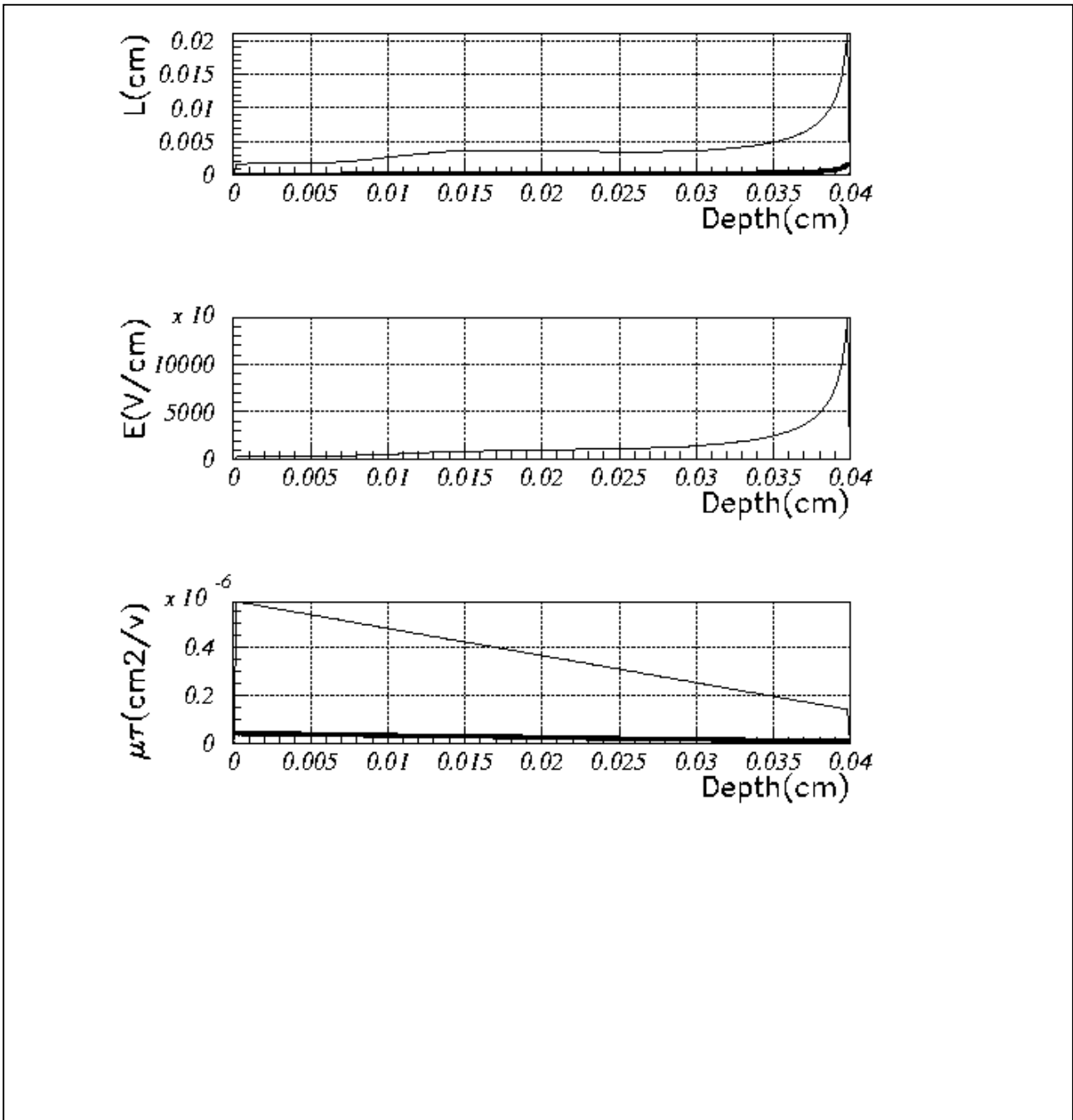


Fig. 27 – Results from the fit applied to data of Fig. 26 :

Top : collection length profile for electrons (continuous line) and holes (open dots).

Centre : electric field profile

Bottom : (mobility)x(lifetime) profile for electrons (continuous line) and holes (open dots)